Dynamic Modeling of Microalgal Production in Photobioreactors

I. Fernández, J.L. Guzmán, M. Berenguel and F.G. Acién

Abstract In this chapter, dynamic models for microalgal production in open and closed photobioreactors are presented. These models are first principle-based models, which take into account both spatial and temporal gradients for the main culture variables. Both fluid dynamics and biological phenomena are considered in the model equations. Calibration and validation tests are summarized in real open and closed tubular industrial photobioreactors, obtaining successful results. Finally, in view of the obtained results, conclusions about the capabilities of the developed models are drawn, as well as its main uses and applications.

1 Introduction

Microalgae production systems are being globally studied due to their high potential in different industrial fields. Microalgae can be used to develop bioproducts such as pharmaceuticals, cosmetics, animal feeds, etc. (Koller et al. 2014; Spolaore et al. 2006). Furthermore, since microalgae have a high combustion power, they have been classified as the third-generation biofuels, belonging to the renewable energy framework. On the other hand, thanks to CO_2 fixation that is performed by their cells during the photosynthetic process, these production systems allow to mitigate the greenhouse gases emission generated by other industrial processes, and they can be

I. Fernández · J.L. Guzmán (✉) · M. Berenguel
Department of Informatics, University of Almería, ceiA3,
CIESOL, Almería, Spain
e-mail: joguzman@ual.es; joseluis.guzman@ual.es

I. Fernández
e-mail: ifernandez@ual.es

M. Berenguel
e-mail: beren@ual.es

F.G. Acién
Department of Chemical Engineering, University of Almería, ceiA3,
CIESOL, Almería, Spain
e-mail: facien@ual.es

B.N. Tripathi and D. Kumar (eds.), *Prospects and Challenges in Algal Biotechnology*, DOI 10.1007/978-981-10-1950-0_2

even used in wastewater treatment processes. Usually, two types of photobioreactors are mainly used to produce microalgae: (i) closed photobioreactors as tubular or flat panels reactors, in which high-value products are produced by strains highly sensitive to contamination; and (ii) open reactors as open ponds and raceway reactors, simpler and less-expensive ones where contamination-proof strains can be produced (Acién et al. 2013; Posten 2009).

Nowadays, an important effort is being performed to introduce this microalgae-based technology in the energy market. Nevertheless, it is necessary to reduce costs and to guarantee that the production from the microalgae culture is performed in a controlled way with the best efficiency as possible. Therefore, the biomass production must be increased while at the same time the associated cost must be reduced in large-scale facilities. Optimization methodologies based on modeling and control approaches are becoming the solution to reach these objectives (Andrade et al. 2016).

Currently, from an automatic control and engineering point of view, a large number of applications related to the optimal production of biomass for systems based on microalgae are opened, owing to the lack for this kind of works in the literature (Andrade et al. 2016; Bernard 2011). The main reason of this lack is the absence of dynamic models that describe in an appropriate way the whole phenomena related to the growth and the biomass production. On the other hand, there are few studies related to the culture control conditions or addressed to the global optimization of these production systems from a control point of view (Andrade et al. 2016; Bernard 2011), mainly due to the high complexity of the required models or problems associated with the systems. For all these reasons, the availability of high-quality models for photobioreactors plays a key role in the control design stage for the optimization of the biomass production (Berenguel et al. 2004; García et al. 2003).

Nonlinear dynamic models are rarely found to represent the microalgal production processes based on photobioreactors. The main reason is because microalgae are photosynthetic organisms that are difficult to manage and use as they have a strong aptitude to store nutrients. Second, their pigments attenuate the light, which is their source of energy and this generates a strong coupling between biology (microalgae growth) and physics (radiative transfer properties and hydrodynamics). Finally, such organisms are most of the time far from the classical hypotheses (namely balanced growth) required to apply classical results in metabolic engineering. For that reason, most existing models describe separately some of these processes (Acién et al. 1998; Concasa et al. 2010), or considering steady-state balances where the reactor has been analyzed as a stirred tank reactor (Guterman et al. 1990; James and Boriah 2010; Jupsin et al. 2003; Xin et al. 2010).

Therefore, dynamic models that take into account the temporal–spatial distribution of culture parameters are necessary to adequately simulate this type of reactors. Moreover, these dynamic models are necessary to optimize the design and operation of the systems, helping to understand the different dynamics and phenomena taking place. Furthermore, these models can be used as predictive and simulation tools in order to properly design and operate these systems, as well as to design control

strategies for optimal biomass production such as pointed out above (Acién et al. 2013; Norsker et al. 2011).

This chapter presents two dynamic model of microalgae production in both tubular and raceway reactors (Fernández et al. 2014, 2016). The models are based on mass balances, transport phenomena, thermodynamic relationships, and biological phenomena taking place in the reactors, thus being based on fundamental principles instead of empirical equations. They take into account the kinetics of different phenomena inside the reactor, and thus a complete dynamic simulation model can be obtained. The models allow predicting the evolution of the main variables of the system such as biomass concentration, pH, dissolved oxygen, and total inorganic carbon in the liquid phase, in addition to oxygen and carbon dioxide exchange for the gas phase. Both models were calibrated and validated using experimental data from pilot-scale industrial reactors, resulting in powerful tools for the optimization of design/operation of this type of photobioreactors as well as for control design purposes.

2 Materials and Methods

This section summarizes the facilities and materials used for the experiments presented in this chapter.

2.1 Closed Tubular Photobioreactor

2.1.1 Microorganism and Culture Medium

The strain selected to be cultivated into the tubular photobioreactor was *Scenedesmus almeriensis* (CCAP 276/24, Culture collection of Algae and Protozoa of the Center for Hydrology and Ecology, Ambleside, UK). This strain stands temperature up to 45 °C and pH values up to 10, being its optimum conditions of 35 °C and pH 8 (Sánchez et al. 2008a, b). The experiments performed in this work took place in a tubular photobioreactor manipulated in continuous mode at a dilution rate of 0.34 1 day^{-1}. The culture medium was Mann & Myers, prepared using agricultural fertilizers instead of pure chemicals. The microalgae were grown photoautotrophically with a continuous aeration to avoid dissolved oxygen accumulation, under pH and temperature-controlled conditions.

2.1.2 Tubular Reactor and Operation Conditions

Experiments were performed on a tubular photobioreactor which belongs to a microalgal production facility, which is situated inside a greenhouse and located at research center “Estación Experimental Las Palmerillas”, property of CAJAMAR Foundation (Almería, Spain). Ten tubular fence-type photobioreactors were built as

described in Acién et al. (2001) and Molina et al. (2001). Figure 1 shows a view of this facility. The photobioreactor can be divided into two main parts (see Fig. 2). On one hand, the solar receiver is designed to maximize the interception of solar radiation, minimizing resistance to flow, and occupying the minimum area as much as possible. On the other hand, a bubble column is used for mixing, degassing, and heat exchange culture. The total culture volume is 2600 l; the photobioreactor has 19.0 m length and 0.7 m width. The solar receiver is made of transparent tubes joined into a loop configuration to obtain a total horizontal length of 400 and 0.09 m diameters. The microalgal culture is circulated at 1 m s^{-1} using a centrifugal pump located between the bubble column and the solar receiver. The pH of the culture is controlled by on-demand injection of pure CO_2 at 5 l min^{-1}. The bubble column has 3.2 m height and 0.4 m inner diameter, and the dissolved oxygen is removed by a constant airflow rate of 140 l min^{-1}. Furthermore, the culture temperature is controlled through an internal heat exchanger located at the bubble column by passing cooling water at 1500 l h^{-1}. The culture is harvested at an overflow at the top of the column when freshwater is poured into the bubble column. Moreover, the pH, temperature, and dissolved oxygen are measured at several positions (3 for dissolved oxygen: at the bottom, middle, and top of the photobioreactor; and 5 for pH and temperature from the bottom to the top of the photobioreactor, being evenly distributed) along the tube using Crison probes (Crison Instru-

Fig. 1 Real view of the tubular photobioreactor at the experimental station

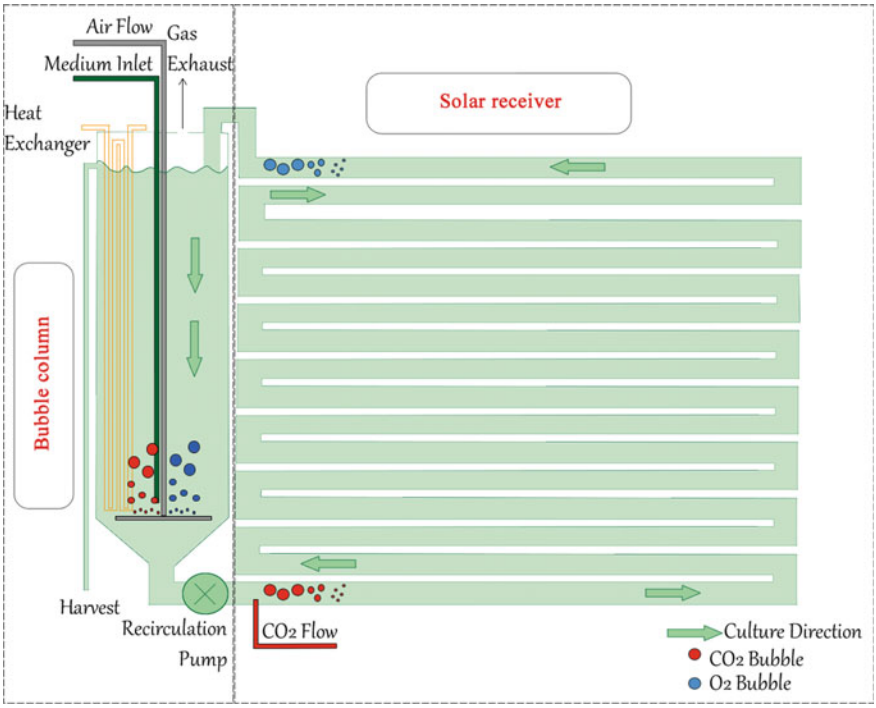

Fig. 2 Tubular photobioreactor scheme

ments, Spain), connected to a control transmitter unit MM44 (Crison Instrument, Spain); liquid and gas flow rates are measured using digital flow meters (PF2W540 and PF2A510, from SMC, Japan). All of these measures are in turn connected to a control computer through a data acquisition device NI Compact FieldPoint (National Instruments, USA). The complete system was designed and built by the Department of Chemical Engineering at the University of Almería (Spain), the control and data acquisition system was developed by the Department of Informatics at the University of Almería (Spain) using the development framework NI Labview (LabVIEW 2011 National Instrument, USA).

2.2 Raceway Photobioreactor

2.2.1 Microorganism and Culture Medium

As for the tubular photobioreactor, the microalgae strain used was *Scenedesmus almeriensis* (CCAP 276/24). However, in this case, experiments were performed using Arnon medium prepared with fertilizers instead of pure chemicals.

Fig. 3 Real view of the raceway reactor at the experimental station

2.2.2 Raceway Reactor and Operation Conditions

The raceway reactor used is located at 36° 48'N–2°43' W and also in Research Center "Las Palmerillas", property of Cajamar Foundation (Almería, Spain). The reactor consisted of two 50-m-length channels (0.46 m high × 1 m wide), both of them connected by 180° bends at each end, with a 0.59 m3 sump (0.65 m long × 0.90 m wide × 1 m deep) located 1 m part of the way down one channel (see Figs. 3 and 4). The entire reactor, including the sump, was made of white 3-mm-thick fiberglass. The liquid was circulated by a marine plywood paddle wheel with eight paddles, with a 1.2 m diameter, which is driven by an electric motor (Ebarba, Barcelona, Spain) with gear reduction and speed control using a frequency inverter (Ibérica, S.A. Barcelona, Spain). The reactor can be divided into three main parts depending on its fluid dynamic characteristics (channels, paddle wheel, and sump), such as observed in Fig. 4. For this reason, three pH-T and dissolved oxygen probes were situated at the end of each of these parts (5083T and 5120, Crison, Barcelona, Spain), connected to transmitters (MM44, Crison, Barcelona, Spain) and data acquisition software (Labview, National Instruments, USA). Air or CO_2 gas was automatically injected at the bottom of the sump through a diffuser to control the dissolved oxygen and pH of the culture. The gas flow rate entering to the reactor was measured by a mass flow meter (PFM 725S-F01-F, SMC, Tokyo, Japan).

Experiments were performed in semicontinuous mode. For this purpose, the reactor was filled with Arnon medium up to 15 cm water depth (15 m^3 volume), prepared from fertilizers instead of pure chemicals, and it was inoculated with a 10% total volume of culture from a 3.0 m^3 tubular photobioreactor. Then, it was operated in batch mode for 1 week. After that, the reactor was operated in semicontinuous mode at

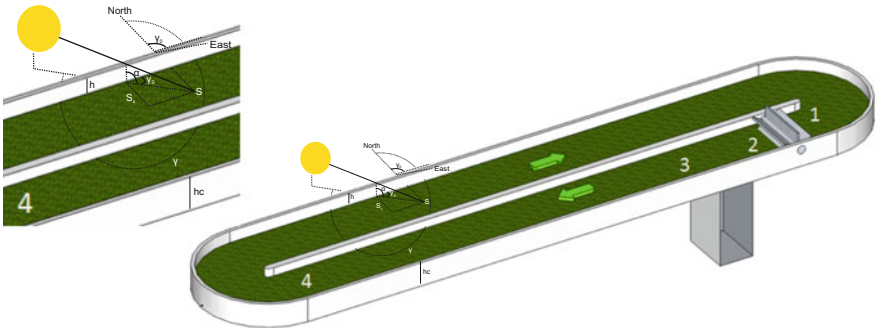

Fig. 4 Raceway reactor scheme showing dimensions. Numbers indicate the position where the probes were situated. (1) before paddle wheel, (2) after paddle wheel—before sump, (3) after sump—beginning of the channel, (4) end of the right channel

0.2 day^{-1}, this being previously demonstrated as optimal for this reactor (Mendoza et al. 2013b). To operate in semicontinuous mode, a fixed culture volume of 3.0 m^3 was harvested and replaced daily with the fresh medium over 6 h in the middle of the daylight period. Semicontinuous operation was maintained till steady state was achieved; only data around steady-state conditions being used. Evaporation (6–10 L/m^2 day^{-1}) inside the reactors was compensated by adding fresh medium, in addition to the volume of fresh medium used for the reactor' semicontinuous operation. The culture medium was not sterilized, simply filtered before entering the reactors using 200 μm pore-size filters to remove solids.

3 Dynamic Models

This section presents the nonlinear dynamic models for both tubular and raceway reactors. These models combine the fluid dynamic and mass transfer capacity of the reactors with the biological performance of the cells under different conditions. The models are based on mass balances, transport phenomena, thermodynamic relationships, and biological phenomena taking place into the system. Both models have been developed following the same ideas, since most of the physical–chemical balances are very similar in tubular and raceway reactors. So, temporal and spatial behaviors of the main variables of the system (such as biomass concentration, pH, dissolved oxygen, and total inorganic carbon in the liquid phase, in addition to oxygen and carbon dioxide exchange for the gas phase) are derived from the corresponding equations.

3.1 Modeling Issues

Microalgae cultures are composed of liquids, gases, and single-cell phototrophic microorganisms (considered as part of the liquid fraction of the system), whose productivity depends on the culture conditions to which the cells are exposed. Therefore, the first principle-based model must represent the physicochemical and biological phenomena that take place in the system, taking into account the relationships between light availability, culture conditions, and photosynthesis rate, besides the mixing and gas–liquid mass transfer inside the system. In outdoor cultures, the solar irradiance and temperature available depend on the location of the photobioreactor, while the rest of nutrients needed for the cells depend on design and operating conditions of the photobioreactor. Thereby, a general growth model for microalgal production system can be developed irrespective of photobioreactor type. Growth can be modeled by a function of the photosynthesis rate. The main parameter that determines the photosynthesis rate is the available light, based on external irradiance, culture characteristics, and reactor geometry (Acién et al. 1999, 2013). Thus, this fact will be first analyzed for each type of reactor to be related with the photosynthesis rate. Afterward, mass balances in liquid and gas states will be presented proving both spatial and temporal gradients for the main culture variables (Fernández et al. 2014, 2016).

3.2 Model for Tubular Photobioreactor

For the tubular reactor, the available light is calculated as a function of the total incident radiation on the photobioreactor surface, the light attenuation by biomass (Beer-Lambert law), and integrating local values over the total culture volume (Molina et al. 1996). However, bearing in mind a specific geometry and photobioreactor, this function can be simplified by Eq. (1) (Acién et al. 1997; Molina et al. 1996):

$$I_{av}(t,x) = \frac{I_0(t)\alpha_t}{K_{a,t}C_b(t,x)d_{t,p}}(1 - exp(-K_{a,t}C_b(t,x)d_{t,p})), \tag{1}$$

where t is the time, x is the space, I_0 is the solar irradiance on an obstacle-free horizontal surface, $K_{a,t}$ is the extinction coefficient, C_b is the biomass concentration, and $d_{t,p}$ is the tube diameter in the p part (where p can be substituted by l for the loop—solar receiver—and c for the bubble column). The solar irradiance has been modulated by a distribution factor α_t, which represents the solar irradiance fraction available in the particular area of the reactor.

The available average irradiance is correlated with the photosynthesis rate by a hyperbolical function as proposed in Costache et al. (2013), Molina et al. (1996a, b). This function is completed in this work by adding the rest of factors that limit the microalgal growth (under sufficient conditions of nutrients). So, the influences of the

pH culture value and dissolved oxygen of the culture have been modeled as described in Costache et al. (2013). Thus, a potential equation describes the influence of dissolved oxygen concentration on the photosynthesis rate, whereas for the temperature and pH conditions two models based on the Arrhenius equation were selected. The complete version for the photosynthesis rate is described by Eq. (2):

$$P_{O_{2,t}}(t,x) = \frac{P_{O_{2,max,t}} I_{av}(t,x)^{n_t}}{K_i exp(I_{av}(t,x)m_t) + I_{av}(t,x)^{n_t}} \left(1 - \left(\frac{[O_2](t,x)}{K_{O_2,t}}\right)^z\right) \left(B_1 exp\left(\frac{-C_1}{pH(t,x)}\right) - B_2 exp\left(\frac{-C_2}{pH(t,x)}\right)\right) - rP_{O_{2,max,t}}, \tag{2}$$

where $P_{O_{2,t}}$ is the photosynthesis rate (oxygen production rate per biomass mass unit), $P_{O_{2,max,t}}$ is the maximum photosynthesis rate for microorganisms under the culture conditions, $[O_2]$ is the dissolved oxygen concentration in liquid phase, n_t is the form exponent, and the term in the denominator is the irradiance constant, which increases as an exponential function of average irradiance, K_i and m_t being form parameters of this relationship, $K_{O_2,t}$ is the oxygen inhibition constant, and z is a form parameter. For the pH influence on the photosynthesis rate, B_1 and B_2 are the pre-exponential factors and C_1 and C_2 are the activation energies of the Arrhenius model. Furthermore, a factor r was included for the respiration phenomenon based on maximum photosynthesis rate.

On the other hand, the carbon dioxide uptake, $P_{CO_{2,t}}$, can be expressed as a one-to-one molar ratio between oxygen and carbon dioxide as follows:

$$P_{CO_{2,t}}(t,x) = -P_{O_{2,t}}(t,x). \tag{3}$$

While the biological phenomena are represented by the equations described above, the mixing, the gas–liquid mass transfer, and the heat transfer are explained in the next section. The balances, for the solar receiver, are formulated by means of several Partial Differential Equations (PDE) that lead to a distributed description of the process in the form of plug flow (approximation that allows to find a tradeoff between model performance and computational cost). On the other hand, the bubble column is considered as stirred tank perfectly mixing, being able to model it by Ordinary Differential Equations (ODE), although a plug flow approach can be also used.

3.2.1 Engineering Model of the Reactor

Tubular photobioreactors are composed of different parts: a solar receiver and a mixing unit, where the culture being recirculated from one to the other continuously using either airlift or mechanical pumps (see Fig. 2). The model of these processes must be applied to these different zones, since the mass transfer and fluid dynamics in each part are different, with variation for the position and time taking place in

each of them. Usually, the mixing unit is usually a bubble column, whereas the solar receiver is a continuous external tubular loop. In the bubble column, air is supplied for oxygen desorption, the liquid phase circulating through the column from the outlet to the inlet of the solar receiver. Thus, in this case, perfect mixing is considered to occur for both the liquid and gas phases. In the loop, the liquid is circulated by a centrifugal pump with pure CO_2 gas being supplied on demand for pH control. Therefore, plug flow has to be considered for the liquid and gas phases, and thus the external loop being divided into differential elements in which perfect mixing is assumed. The total number of differential elements is a function of the dispersion coefficient or mixing in the system (determined experimentally) (Fernández et al. 2012, 2014).

3.2.2 Mass Balances in the Liquid Phase

A mass balance for the biomass concentration can be defined as in Eq. (4), taking into account the photosynthesis process performed by the microalgae culture, and the transport phenomena due to the recirculation of the culture along the photobioreactor,

$$A_{liq,l}(t,x)\frac{\partial C_b(t,x)}{\partial t} = -Q_{liq,l}(t,x)\frac{\partial C_b(t,x)}{\partial x} + A_{liq,l}(t,x)P_{O_{2,t}}(t,x)C_b(t,x)Y_{o/x}, \tag{4}$$

where the subindex l refers to the solar receiver, $A_{liq,l}$ is the cross-sectional liquid area in the solar receiver that can be calculated as $A_{t,l}(1-\varepsilon_l(t,x))$, with $A_{t,l}$ being the total cross-sectional area of the loop and ε_l is the gas holdup, $Q_{liq,l}$ is the volumetric flow rate of liquid defined as $VA_{liq,l}$, where $V(t)$ is the velocity of the fluid established by the centrifugal pump of the photobioreactor, and $Y_{o/x}$ is the biomass yield coefficient produced by the oxygen unit mass.

In the bubble column, a similar balance can be considered by an ordinary differential equation where the spatial dimension is removed (although as has been pointed before, plug flow could also be considered). Furthermore, since the dilution process is performed in this part of the photobioreactor, an output biomass concentration has been added driven by the volumetric flow rate of medium, Eq. (5).

$$V_{liq,c}(t)\frac{dC_{b,out}(t)}{dt} = -Q_{liq,c}(t)(C_{b,out}(t) - C_{b,in}(t)) + V_{liq,c}(t)P_{O_{2,t}}(t)C_{b,out}(t)Y_{o/x} - Q_m(t)C_{b,out}(t), \tag{5}$$

where the subindex c refers to the bubble column, $V_{liq,c}$ is the liquid volume, which can be calculated as $V_{t,c}(1-\varepsilon_c(t))$ where $V_{t,c}$ is the total volume and ε_c is the gas holdup, $Q_{liq,c}$ is the volumetric flow rate of liquid, $C_{b,out}$ is the outlet biomass concentration (solar receiver input), $C_{b,in}$ is the inlet biomass concentration (solar receiver output), and Q_m is the volumetric flow rate of culture medium.

Regarding dissolved oxygen concentration, it can be related to the gas–liquid mass transfer rate and the photosynthesis rate by the following mass balance:

$$A_{liq,l}(t,x)\frac{\partial[O_2](t,x)}{\partial t} = -Q_{liq,l}(t,x)\frac{\partial[O_2](t,x)}{\partial x} + A_{liq,l}(t,x)\frac{P_{O_{2,t}}(t,x)C_b(t,x)}{M_{O_2}} + A_{liq,l}(t,x)K_l a_{l,O_2 l}(t,x)([O_2^*](t,x) - [O_2](t,x)), \tag{6}$$

where $[O_2]$ is the dissolved oxygen concentration in liquid phase, M_{O_2} is the molecular weight of oxygen, $K_l a_{l,O_2 l}$ is the volumetric gas–liquid mass transfer coefficient for oxygen, and $([O_2^*] - [O_2])$ is the mean driving force. The equilibrium concentration in gas phase $[O_2^*]$ is calculated as a function of the oxygen concentration in the gas phase based on Henry's law by Eq. (7):

$$[O_2^*](t,x) = H_{O_2} P_T y_{O_2}(t,x), \tag{7}$$

where H_{O_2} is the Henry's constant for oxygen, P_T is the total pressure, and y_{O_2} is the oxygen molar fraction in the gas phase.

The homologous balance for the bubble column must consider the dissolved oxygen concentration in the input medium liquid. Thus, the next balance can be established as

$$V_{liq,c}(t)\frac{d[O_2]_{out}(t)}{dt} = -Q_{liq,c}(t)([O_2]_{out}(t) - [O_2]_{in}(t)) + V_{liq,c}(t)\frac{P_{O_{2,t}}(t)C_{b,out}(t)}{M_{O_2}} + V_{liq,c}(t)K_l a_{l,O_2 c}(t)([O_2^*](t) - [O_2](t))_{ml} - Q_m(t)([O_2]_{m,t} - [O_2]_{out}(t)), \tag{8}$$

where $[O_2]_{in}$ and $[O_2]_{out}$ are the oxygen concentrations in liquid phase at the inlet and outlet of the bubble column, $K_l a_{l,O_2 c}$ is the volumetric gas–liquid mass transfer coefficient for oxygen in the bubble column, $([O_2^*] - [O_2])_{ml}$ is a logarithmic mean driving force, and $[O_2]_{m,t}$ is the dissolved oxygen in the culture medium.

Regarding inorganic total carbon concentration, it can be calculated by a mass balance to the liquid phase in a similar way to dissolved oxygen by Eq. (9):

$$A_{liq,l}(t,x)\frac{\partial[C_T](t,x)}{\partial t} = -Q_{liq,l}(t,x)\frac{\partial[C_T](t,x)}{\partial x} + A_{liq,l}(t,x)\frac{PCO_{2,t}(t,x)C_b(t,x)}{M_{CO_2}} + A_{liq,l}(t,x)K_l a_{l,CO_2 l}(t,x)([CO_2^*](t,x) - [CO_2](t,x)), \tag{9}$$

where $K_l a_{l,CO_2 l}$ is the mass transfer coefficient for CO_2, and total inorganic carbon in the liquid phase is defined as $[C_T]$, which depends on the carbon dioxide concentration in the liquid phase $[CO_2]$ and the equilibrium concentration in the gas phase $[CO_2^*]$. The equilibrium concentration can be calculated, according to Henry's law, as a function of Henry's constant, H_{CO_2}, the total pressure P_T and the molar fraction of CO_2 in the gas phase, y_{CO_2}.

For the bubble column, the inorganic carbon concentration from culture medium must be regarded in the balance as shown in Eq. (10):

$$\begin{aligned} &V_{liq,c}(t)\frac{d[C_T]_{out}(t)}{dt} = -Q_{liq,c}(t)([C_T]_{out}(t) - [C_T]_{in}(t)) + \\ &V_{liq,c}(t)\frac{P_{CO_{2,t}}(t)C_{b,out}(t)}{M_{CO_2}} + V_{liq,c}(t)K_l a_{l,CO_2 c}(t)([CO_2^*](t) - [CO_2](t))_{lm} - \\ &Q_m(t)([C_T]_{m,t} - [C_T]_{out}(t)), \end{aligned} \tag{10}$$

where $K_l a_{l,CO_2 c}$ is the mass transfer coefficient for CO_2 in the bubble column. The total inorganic carbon is defined at the inlet $[C_T]_{in}$ and outlet $[C_T]_{out}$ of the bubble column, and $[C_T]_{m,t}$ is the inorganic carbon concentration in the culture medium.

The pH value is defined as the decimal logarithm of the hydrogen concentration in the system, $-log10([H^+])$. Several equilibrium relations can be found between the hydrogen concentration and carbon species in the system (dissolved carbon dioxide, carbonate, $[HCO_3^-]$, and bicarbonate, $[CO_3^{2-}]$) as can be seen in Fernández et al. (2012).

3.2.3 Mass Balances in the Gas Phase

In addition to the liquid phase, CO_2 injections in gaseous form are incorporated in order to adjust the pH and neutralize the carbon lack in the system during photosynthesis process. On the other hand, air injections are demanded in the bubble column to control high levels of dissolved oxygen accumulated into the loop. Therefore, mass balances on the gas phases are needed to include these phenomena. Since the nitrogen molar fraction can be considered constant because its solubility is approximately zero, the balances presented here are formulated by relations from the rest of gases to nitrogen molar ratio. Regarding the oxygen, the next balance, Eq. (11), can be established:

$$\begin{aligned} &A_{gas,l}(t,x)\frac{\partial Y_{O_2}(t,x)}{\partial t} = -\frac{F_{N_{2,l}}(t,x)V_{mol}}{y_{N_{2,l}}}\frac{\partial Y_{O_2}(t,x)}{\partial x} - \\ &\frac{A_{liq,l}(t,x)V_{mol}}{y_{N_{2,l}}}K_l a_{l,O_2 l}(t,x)([O_2^*](t,x) - [O_2](t,x)), \end{aligned} \tag{11}$$

where $A_{gas,l}$ is the cross-sectional gas area, which can be calculated as $A_{t,l}\varepsilon_l(t,x)$, V_{mol} is the molar volume under reactor conditions (pressure and temperature), Y_{O_2} is the oxygen-to-nitrogen molar ratio in the gas phase, $F_{N_{2,l}}$ is the molar flow rate of nitrogen in the gas phase, and $y_{N_{2,l}}$ is the nitrogen molar fraction used in the solar receiver. For the column, a similar mass balance can be considered taking into account the gas characteristics injected in this section. Thus, an ODE can be written as shown in Eq. (12):

$$V_{gas,c}(t)\frac{dY_{O_2,out}(t)}{dt} = -\frac{F_{N_{2,c}}(t)V_{mol}}{y_{N_{2,c}}}(Y_{O_2,out}(t) - Y_{O_2,in}(t)) - \frac{V_{liq,c}(t)V_{mol}}{y_{N_{2,c}}}K_l a_{l,O_2c}(t)([O_2^*](t) - [O_2](t))_{lm}, \tag{12}$$

where the oxygen-to-nitrogen molar ratio in the gas phase is defined at the inlet $Y_{O_2,in}$ and outlet $Y_{O_2,out}$ of bubble column, $V_{gas,c}$ is the gas volume, which can be calculated as $V_{t,c}\varepsilon_c(t)$, $F_{N_{2,c}}$ is the molar flow rate of nitrogen for the bubble column, and $y_{N_{2,c}}$ is the nitrogen molar fraction used in the bubble column. For the carbon dioxide, an analogous mass balance can be defined by Eq. (13):

$$A_{gas,l}(t,x)\frac{\partial Y_{CO_2}(t,x)}{\partial t} = -\frac{F_{N_{2,l}}(t,x)V_{mol}}{y_{N_{2,l}}}\frac{\partial Y_{CO_2}(t,x)}{\partial x} - \frac{A_{liq,l}(t,x)V_{mol}}{y_{N_{2,l}}}K_l a_{l,CO_2l}(t,x)([CO_2^*](t,x) - [CO_2](t,x)), \tag{13}$$

where Y_{CO_2} is the carbon dioxide to nitrogen molar ratio in the gas phase, $F_{N_{2,l}}$ is the molar flow rate of nitrogen in the gas phase, and $y_{N_{2,l}}$ is the nitrogen molar fraction used in the solar receiver. The perfectly mixing version for the bubble column is represented by Eq. (14):

$$V_{gas,c}(t)\frac{dY_{CO_2,out}(t)}{dt} = -\frac{F_{N_{2,c}}(t)V_{mol}}{y_{N_{2,c}}}(Y_{CO_2,out}(t) - Y_{CO_2,in}(t)) - \frac{V_{liq,c}(t)V_{mol}}{y_{N_{2,c}}}K_l a_{l,CO_2c}(t)([CO_2^*](t) - [CO_2](t))_{lm}, \tag{14}$$

where the carbon dioxide to nitrogen molar ratio in the gas phase is defined at the inlet $Y_{CO_2,in}$ and outlet $Y_{CO_2,out}$ of bubble column.

In both mass balances, molar ratio to nitrogen is used instead of molar fraction. However, a relationship between these units is known by Eq. (15):

$$y = \frac{Y}{1+Y}. \tag{15}$$

An improvement has been developed taking into account the nitrogen gas transport since, although this element can be constant due to lack of mass transfer, a transport effect is produced when a gas bubble is injected in the loop up to finally leaves it. Assuming the same velocity for each component of the gas flow rate and no slip between the liquid phase and the gas phase, the gas transport can be modeled by changes in the cross-sectional area of the nitrogen A_{N_2} along the tube, being able to describe these changes by the following balance:

$$A_{gas,l}(t,x)\frac{\partial A_{N_{2,l}}(t,x)}{\partial t} = -\frac{F_{N_{2,l}}(t,x)V_{mol}}{y_{N_{2,l}}}\frac{\partial A_{N_{2,l}}(t,x)}{\partial x}, \tag{16}$$

where $A_{N_{2,l}}$ is the cross-sectional area of the nitrogen in the solar receiver.

A relation can be found between the molar flow rate of nitrogen and the gas flow rate along the tube by Eq. (17):

$$F_{N_{2,l}}(t,x) = \frac{Q_{gas,l}(t,x)y_{N_{2,l}}}{V_{mol}}, \tag{17}$$

where the volumetric flow rate of gas $Q_{gas,l}$ can be established as the sum of the three volumetric flow rates which take place into the loop (carbon dioxide, oxygen, and nitrogen). Therefore, a relationship between the volumetric flow rate of gas and the cross-sectional nitrogen area can be calculated using the molar ratio to nitrogen for the rest of components as

$$Q_{gas,l}(t,x) = VA_{N_{2,l}}(t,x)(1 + Y_{O_2}(t,x) + Y_{CO_2}(t,x)). \tag{18}$$

On the other hand, the gas holdup determines the mass transfer in both the bubble column and the solar receiver. Bearing in mind physical characteristics of each part of the system, different models of the gas holdup were modeled. For the solar receiver, assuming no slip between the liquid phase and the gas phase, the gas holdup expression can be approximated by Eq. (19):

$$\varepsilon_l(t,x) = \frac{Q_{gas,l}(t,x)}{Q_{gas,l}(t,x) + Q_{liq,l}(t,x)}. \tag{19}$$

In the bubble column, a slip velocity exits between the gas and the liquid phases. Therefore, a drift flux model can be used to predict the gas holdup (Zuber and Findlay 1965), which is given by Eq. (20):

$$\varepsilon_c(t) = \frac{U_{gas}(t)}{(C_o U_{gas}(t) + U_{liq}(t)) + U_\infty}, \tag{20}$$

where U_{gas} and U_{liq} are the superficial velocity of the gas and liquid, respectively. C_o is a drift flux model parameter and U_∞ is the bubble accession rate.

Therefore, the mass transfer coefficient can be defined as a function of the gas holdup according to the part of the system that is modeled (Chisti and Moo-Young 1987). Even further, the mass transfer coefficient for the CO_2 is directly related to the mass transfer coefficient for the oxygen by the difference in aqueous diffusivity of the two gases (K_{CO_2}) as follows (Molina et al. 1993), Eqs. (21) and (22):

$$K_l a_{l,O_2 l}(t,x) = a_l \varepsilon_l(t,x)^{b_l} \qquad K_l a_{l,CO_2 l}(t,x) = K_{CO_{2,l}} K_l a_{l,O_2 l}(t,x) \tag{21}$$

$$K_l a_{l,O_2 c}(t) = a_c \varepsilon_c(t)^{b_c} \qquad K_l a_{l,CO_2 c}(t) = K_{CO_{2,c}} K_l a_{l,O_2 c}(t). \tag{22}$$

$K_{CO_{2,l}}$ and $K_{CO_{2,c}}$ are the transfer coefficient constants for CO_2 at the solar receiver and at the bubble column, respectively; whereas a_l, b_l and a_c, b_c are form parameters adjusted to each part of the photobioreactor.

Another possible characterization of the mass transfer coefficients can be given by relating the volumetric interfacial area, Eq. (23), between the gas and the liquid phases:

$$K_l a_{l,O_2}(t,x) = K_l a_i(t,x), \tag{23}$$

where K_l is the liquid-side mass transfer coefficient, and a_i is the interfacial area which can be calculated by the initial bubble diameter, d_b, and the gas holdup in each loop section as

$$a_i(t,x) = \frac{6\varepsilon_l(t,x)}{d_b(1-\varepsilon_l(t,x))}. \tag{24}$$

3.3 Model for Raceway Photobioreactor

Such as mentioned above, the solar radiation availability is the first element to be analyzed when a model of this type is developed. For the raceway reactor (as horizontal surface), light availability can be easily estimated using classical solar radiation equations. However, the net amount of light received in raceway reactors is a function of its design, especially the walls shadow having a large influence. In this sense, shadow is generated by the channel walls in each cross-sectional area of the reactor, depending on the sun position and reactor geometry. Therefore, shadow influences the photosynthesis rate, and it can be modeled as a distributed factor (α_s) in each cross-sectional area. The shadow factor (α_s) is calculated taking into account the length of the shadow projection on the perpendicular axis of the walls, such as shown in Fig. 4, using Eqs. (25) and (26) (Kittler and Darula 2013). According to these equations, azimuth (α) and altitude angles (γ) are calculated as a function of the latitude (ϕ), hour angle (ω), and sun declination (δ), these last two terms being a function of the day of the year (N) and the solar hour (h_s). The projection of the shadow generated by the channel walls onto the surface of the cross-sectional area (s_x) can be described in terms of the wall height (h_w), the solar altitude angle, the Azimuth angle, and the angle measured from the North to the normal vector of the cross-sectional area of the reactor (γ_0), in this case 84° (Fig. 4). Finally, the distributed parameter is calculated as the ratio to the total width of the channel as follows:

$$\alpha = \sin^{-1}(\sin(\delta)\sin(\phi) + \cos(\delta)\cos(\phi)\cos(\omega)) \tag{25}$$

$$\gamma = \cos^{-1}\left(\frac{\sin(\delta)\cos(\phi) - \cos(\delta)\cos(\omega)\sin(\phi)}{\cos(\alpha)}\right) \tag{26}$$

$$\begin{aligned} &\text{if } \sin(\omega) > 0 \text{ then } \gamma = 360 - \gamma \\ &\text{if } \sin(\omega) \leq 0 \text{ then } \gamma = \gamma \end{aligned} \tag{27}$$

$$\delta = 23.45 \sin\left(\frac{360(284 + N)}{365}\right) \tag{28}$$

$$\omega = 15(12 - h_s) \tag{29}$$

$$s_x = \text{abs}\left(\frac{(h_w - h) * \sin(\gamma - (180 + \gamma_0))}{tan(\alpha)}\right) \tag{30}$$

$$\alpha_s = \frac{s_x}{w}. \tag{31}$$

Once the distributed factor, α_s, is estimated, the average irradiance (I_{av}) can be obtained. The average irradiance integrates the local irradiance values inside the culture over the total culture volume, being calculated as a function of the total incident radiation on the photobioreactor surface (I_o), the biomass concentration (C_b), the light attenuation of the biomass ($K_{a,r}$), and the light path or culture depth (h) (Molina et al. 1996a). Taking into account the variation of biomass concentration with time, t, and position along the reactor, x, the average irradiance in whatever section of the reactor can be calculated by Eq. (32):

$$I_{av}(t,x) = \frac{I_0(t)}{K_{a,r}C_b(t,x)h}(1 - exp(-K_{a,r}C_b(t,x)h). \tag{32}$$

The photosynthesis rate ($P_{O_{2,r}}$), defined as the oxygen production rate per biomass mass unit, is correlated with the average irradiance by an hyperbolic function, the response of photosynthesis rate to average irradiance being modulated by adequacy of culture conditions using normalized factors (Costache et al. 2013). A potential equation describes the influence of dissolved oxygen concentration on the photosynthesis rate, whereas for the pH a model based on the Arrhenius equation is used. Thus, under nutrient-sufficient conditions, equation (33) can be used to determine the photosynthesis rate as a function of average irradiance, dissolved oxygen concentration ($[O_2]$), and pH into the culture (Costache et al. 2013). In this equation, several biological parameters specific of microalgae strain and growth status of the cells are included, as the maximum photosynthesis rate under the culture conditions ($P_{O_{2,\max,r}}$), the form exponent (n_r), the irradiance constant (as an exponential function of average irradiance, K_i and m_r), the oxygen inhibition constant ($K_{O_{2,r}}$), a form parameter (z), the pre-exponential factors (B_1, B_2), the activation energies of the Arrhenius model (C_1, C_2), and the constant respiration rate (R_{O_2}):

$$P_{O_{2,r}}(t,x) = (1-\alpha_s)\frac{P_{O_{2,max,r}} I_{av}(t,x)^{n_r}}{K_i exp(I_{av}(t,x)m_r) + I_{av}(t,x)^{n_r}} \left(1 - \left(\frac{[O_2](t,x)}{K_{O_{2,r}}}\right)^z\right) \left(B_1 exp\left(\frac{-C_1}{pH(t,x)}\right) - B_2 exp\left(\frac{-C_2}{pH(t,x)}\right)\right) - \alpha_s R_{O_2}. \quad (33)$$

Once the photosynthesis rate is modeled, Eq. (34) allows determining the biological carbon dioxide uptake ($P_{CO_{2,r}}$) considering a one-to-one molar ratio between oxygen and carbon dioxide (from basic equation of photosynthesis). Moreover, considering a mean value of oxygen coefficient yield ($Y_{b/O2}$), the net production of biomass can be determined by Eq. (35):

$$P_{CO_{2,r}}(t,x) = -P_{O_{2,r}}(t,x) \quad (34)$$

$$P_b(t,x) = Y_{b/O_2}(t,x) P_{O_{2,r}}(t,x). \quad (35)$$

3.3.1 Engineering Model of the Reactor

The raceway reactor used in this work has been previously characterized in both fluid dynamic and mass transfer capacity (Godos et al. 2014; Mendoza et al. 2013a, b). According to this previous knowledge, the reactor can be divided into three main zones: channel, paddle wheel, and sump. The channel performs as a plug flow reactor, thus perfect mixing exits into the cross section of the channel, and axial gradients are considered due to biological and mass transfer phenomena. Biological phenomena (production of oxygen, consumption of inorganic carbon, production of biomass, etc.) take place into the channel, in addition to mass transfer between the culture and the atmosphere (oxygen and carbon dioxide exchange). Paddle wheel performs as stirred tank, thus perfect mixing existing in the liquid phase with no gradients taking place. In this section of the reactor, biological phenomena also take place in addition to mass transfer between liquid and atmosphere. The sump performs also as stirred tank for the liquid, and thus no gradients exist. However, as plug flow for the injected gas is considered, gradients of oxygen and carbon dioxide into the gas phase appear. Inside the sump, the same biological phenomena take place, but the mass transfer is a function of gas phase composition along the sump. Assuming constant velocity (V) and liquid height (h) inside the channel, the volumetric flow rate of liquid (Q_{liq}) is defined as the multiplication of velocity and cross-sectional area of the channel (calculated using the liquid height and the width of the channel, w). This flow rate is constant for the three sections of the reactor. Regarding the mass transfer, it is a function of mass transfer coefficient and driving force in each position, the driving force being a function of the component concentration into the liquid phase and that in equilibrium with the gas phase in contact.

To model the raceway reactor, mass balances have been applied to each reactor section. A model using partial differential equations (PDEs) has been used to cope

with the existence of plug flow behavior in some parts of the reactor. PDEs are used in many physical problems, such as fluid flow, heat transfer, solid mechanics, and biological processes. Only ordinary differential equation (ODE) has been applied to stirred tank sections of the reactor as sump and paddle to reduce the computational effort (Fernández et al. 2016).

3.3.2 Mass Balances in the Liquid Phase

The three main components considered into the liquid phase are biomass concentration (C_b), dissolved oxygen concentration ($[O_2]$), and total inorganic carbon concentration ($[C_T]$). A mass balance is defined for each one of the three components in each section of the reactor. Thus, the proposed balances for each one of the three components are shown in equations (36)–(38):

$$wh\frac{\partial C_b(t,x)}{\partial t} = -whV_r\frac{\partial C_b(t,x)}{\partial x} + whP_{O_2}(t,x)C_b(t,x)Y_{b/O_2} \tag{36}$$

$$\begin{aligned} wh\frac{\partial [O_2](t,x)}{\partial t} &= -whV_r\frac{\partial [O_2](t,x)}{\partial x} + \\ &+ wh\frac{P_{O_{2,r}}(t,x)C_b(t,x)}{M_{O_2}} + whK_{laO_{2_{ch}}}([O_2^*](t,x) - [O_2](t,x)) \end{aligned} \tag{37}$$

$$\begin{aligned} wh\frac{\partial [C_T](t,x)}{\partial t} &= -whV\frac{\partial [C_T](t,x)}{\partial x} + \\ &+ wh\frac{P_{CO_{2,r}}(t,x)C_b(t,x)}{M_{CO_2}} + whK_{laCO_{2_{ch}}}([CO_2^*](t,x) - [CO_2](t,x)). \end{aligned} \tag{38}$$

The oxygen mass transfer is a function of the volumetric coefficient for oxygen into the channel ($K_{laO_{2_{ch}}}$) and the logarithmic driving force ($[O_2^*]-[O_2]$) (Camacho et al. 1999). The dissolved oxygen concentration in equilibrium with air surrounding the channel ($[O_2^*]$) is calculated as a function of the oxygen molar fraction into the air (0.21) based on Henry's law. The carbon dioxide mass transfer is calculated in the same way as a function of volumetric mass transfer for carbon dioxide into the channel ($K_{laCO_{2_{ch}}}$), which could be directly related to $K_{laO_{2_{ch}}}$ by a factor of 0.93, which takes into account the difference in aqueous diffusivity of the two gases. Regarding the carbon dioxide concentration ($[CO_2]$), it is a function of total inorganic carbon ($[C_T]$) and pH, due to the existence of bicarbonate buffer (Camacho et al. 1999). The carbon dioxide concentration in equilibrium with the gas phase ($[CO_2^*]$) is also calculated as a function of the carbon dioxide molar fraction into the air (0.0003) based on Henry's law.

Analogous mass balances are applied to the paddle wheel, considering that this section can be represented by ODEs. For the paddle wheel, the concentration of

the major components at inlet is that calculated as outlet from the channel. Equations (39)–(41) allow us calculating the biomass, dissolved oxygen, and inorganic carbon concentration at the outlet of the paddle wheel taking into account the specific dimensions and mass transfer coefficients in this section. It is important to note that in paddle wheel, air is also the gas in contact with the liquid phase, its concentration being constant in spite of oxygen and carbon dioxide exchange:

$$\frac{dC_{b,out}(t)}{dt} = -\frac{Q_{liq}}{V_p}(C_{b,out}(t) - C_{b,in}(t)) + \\ + P_{O_{2,r}}(t)C_{b,in}(t)Y_{b/O_2} \tag{39}$$

$$\frac{d[O_2]_{out}(t)}{dt} = -\frac{Q_{liq}}{V_p}([O_2]_{out}(t) - [O_2]_{in}(t)) + \\ + \frac{P_{O_{2,r}}(t)C_{b,out}(t)}{M_{O2}} + K_{laO_{2_p}}([O_2^*](t) - [O_2](t))_{lm} \tag{40}$$

$$\frac{d[C_T]_{out}(t)}{dt} = -\frac{Q_{liq}}{V_p}([C_T]_{out}(t) - [C_T]_{in}(t)) + \\ + \frac{P_{CO_{2,r}}(t)C_{b,out}(t)}{M_{CO2}} + K_{laCO_{2_p}}([CO_2^*](t) - [CO_2](t))_{lm}. \tag{41}$$

Similar mass balances are applied to the sump also considering that this section can be represented by ODEs. For the sump, the concentration of major components at inlet is that calculated as outlet from the paddle wheel. Equations (42)–(44) allow us calculating the biomass, dissolved oxygen, and inorganic carbon concentration at the outlet of the sump, respectively:

$$\frac{dC_{b,out}(t)}{dt} = -\frac{Q_{liq}}{V_s(1-\varepsilon_s(t))}(C_{b,out}(t) - C_{b,in}(t)) + \\ + P_{O_{2,r}}(t)C_{b,in}(t)Y_{b/O_2} - \frac{Q_m}{V_s(1-\varepsilon_s(t))}C_{b,out}(t) \tag{42}$$

$$\frac{d[O_2]_{out}(t)}{dt} = -\frac{Q_{liq}}{V_s(1-\varepsilon_s(t))}([O_2]_{out}(t) - [O_2]_{in}(t)) + \\ + \frac{P_{O_{2,r}}(t)Cb_{out}(t)}{M_{O2}} + K_{laO_{2_s}}([O_2^*](t) - [O_2](t))_{lm} + \\ + \frac{Q_m}{V_s(1-\varepsilon_s(t))}([O_2]_m - [O_2]_{out}(t)) \tag{43}$$

$$\frac{d[C_T]_{out}(t)}{dt} = -\frac{Q_{liq}}{V_s(1-\varepsilon_s(t))}([C_T]_{out}(t) - [C_T]_{in}(t)) + \\ + \frac{P_{CO_{2,r}}(t)Cb_{out}(t)}{M_{CO2}} + K_{laCO_{2_s}}([CO_2^*](t) - [CO_2](t))_{lm} + \\ + \frac{Q_m}{V_s(1-\varepsilon_s(t))}([C_T]_{m,r} - [C_T]_{out}(t)). \tag{44}$$

Since air or carbon dioxide is injected into the sump, and the exchange of oxygen and carbon dioxide from the gas phase to the liquid modifies the oxygen and carbon dioxide molar fraction into the gas phase, the oxygen and carbon dioxide in the liquid equilibrium with the gas phase must be dynamically calculated. The outlet of biomass, dissolved oxygen, and inorganic carbon from the system due to harvesting is included by considering the volumetric flow of medium (Q_m). In these equations, the volume of each section is corrected by gas holdup (ε_s) to determine the right liquid volume in each section. The gas holdup can be approximated by Eq. (45) taking into account the difference between the volumetric flow rate of gas introduced in the sump, Q_{gas}, and the total volumetric flow rate of the system (Q_{gas}+Q_{liq}):

$$\varepsilon_s(t) = \frac{Q_{gas}(t)}{Q_{gas}(t) + Q_{liq}(t)}. \tag{45}$$

To apply these equations, the different volumes of each section are considered, and thus the volume of the sump is calculated by Eq. (46) considering the height (h_{ss}), wide (w_s), and length (l_s) of the sump in addition to the volume of channel comprises over the sump:

$$V_s = h_{ss}w_s l_s + hw_s l_s. \tag{46}$$

3.3.3 Mass Balances to the Gas Phase

Air (21% O_2, 0.03% CO_2) or flue gas (6% O_2, 10% CO_2) is injected into the sump to control the dissolved oxygen concentration and the pH of the culture. Thus, when the pH is higher than set point (pH = 8), flue gas is injected to reduce the pH and supply inorganic carbon, otherwise air being injected to minimize the accumulation of dissolved oxygen and to avoid achieving toxic dissolved oxygen concentrations (>250% Sat) (Costache et al. 2013). The injected gas modifies its composition along the sump due to mass transfer, and thus mass balances are also applied to the gas phase to determine its variation along the sump. Since the nitrogen molar flow can be considered constant, because its solubility is low, the balances are formulated by relations from the rest of gases to nitrogen molar ratio. According to Eq. (47), the variation of the oxygen-to-nitrogen molar ratio into the gas phase (Y_{O_2}) is a function of the nitrogen molar fraction into the gas phase (y_{N_2}). For the carbon dioxide,

an analogous mass balance can be defined to determine the variation of the carbon dioxide to nitrogen molar ratio in the gas phase (Y_{CO_2}):

$$\begin{aligned}\frac{dY_{O_2,out}(t)}{dt} &= -\frac{Q_{gas}}{V_s(1-\varepsilon_s(t))}(Y_{O_2,out}(t) - Y_{O_2,in}(t)) \\ &- K_{laO_{2_s}}\frac{V_{mol}}{y_{N_2}}\frac{(1-\varepsilon_s(t))}{\varepsilon_s(t)}([O_2^*](t) - [O_2](t))_{lm}\end{aligned} \tag{47}$$

$$\begin{aligned}\frac{dY_{CO_2,out}(t)}{dt} &= -\frac{Q_{gas}}{V_s(1-\varepsilon_s(t))}(Y_{CO_2,out}(t) - Y_{CO_2,in}(t)) \\ &- K_{laCO_{2_s}}\frac{V_{mol}}{y_{N_2}}\frac{(1-\varepsilon_s(t))}{\varepsilon_s(t)}([CO_2^*](t) - [CO_2](t))_{lm}.\end{aligned} \tag{48}$$

3.4 Solvers and Software

PDEs and ODEs balances, which establish the base of the model, have been implemented by the software Matlab 8.3 (MathWorks, Massachusetts, USA). Since the computational cost required to solve these kinds of equations is high, a general procedure for the first-order hyperbolic equations has been used by means of the well-known method of lines for PDE equations. On the other hand, ODEs balances have been calculated by a forward first-order finite difference approximation method. Note that for the calibration procedure a multidimensional nonlinear minimization process has been formulated, using Sequential Quadratic Programming (SQP) methods since a Quadratic Programming (QP) subproblem was considered. For that reason, an appropriated simulation time of the model is required in order to solve the optimization problem suggested in a reasonable time. Model calibration has been performed comparing real data of pH and dissolved oxygen concentration at the end of the different sections of the reactors, with the simulation response obtained using estimated values of characteristic parameters.

4 Results

This section summarizes the main results obtained for both models. First, calibration and validation results are presented using experimental data, and afterward different analyses are derived by using the resulting models as design/analysis tools (Fernández et al. 2012, 2014, 2016).

The calibration and validation of a biological system is a very complex task due to the large number of experimental tests that must be performed and the number of parameters that have to be calibrated, many of them depending on the culture con-

ditions. For that reason, a suitable methodology is to divide these parameters into different groups depending on their characteristics, for example, biological and fluid dynamic parameters can be separated in order to perform specific tests for each one. Physical and chemical parameters, such as mass and heat transfer coefficients, can be determined by experimental data without culture or using known fluid dynamic relationships (Acién et al. 2001; Camacho et al. 1999). On the other hand, biological parameters can be calculated at laboratory scale, where a lot of conditions can be evaluated, although they must be readjusted in outdoor culture conditions and other scales (Costache et al. 2013; Sánchez et al. 2008a, b). In addition, the whole system can be adjusted from experimental data of outdoor cultures, by fitting these data into the responses of the proposed model. Error metrics, such as integrated absolute error (IAE) or integrated squared error (ISE), can be used for this purpose, formulating an optimization problem for the calibration process. However, the use of experimental data of outdoor cultures must be treated carefully due to different reasons. First, noise and other disturbances must be filtered from the experimental data in order to remove possible uncertainties in the optimization problem. Second, the photosynthesis rate, biological part of the model, is an equation composed by different kinetic equations related to the culture conditions, and thus specific tests must be performed under controlled conditions for an appropriate calibration. However, this process is difficult to carry out in outdoor conditions, and therefore certain constraints and a suitable initial point, based on parameters obtained in laboratory scale, must be established in the calibration problem. Finally, possible disturbances must be considered, above all those affecting the pH variable. Since the pH value is very sensitive to changes in other variables as total inorganic carbon, some disturbances can appear due to inorganic carbon concentration added in the culture medium dilution during the operation in continuous mode, as well as small differences in the mass transfer coefficients because of biological reactions produced during the photosynthesis process.

4.1 Results for Tubular Photobioreactor

This section describes the results obtained for the tubular photobioreactor. From previous works (Camacho et al. 1999; Costache et al. 2013; Mendoza et al. 2013a) and significant knowledge of the processes, experimental data from outdoor culture were only needed to fit the model response from biological parameters obtained in laboratory scale and fluid dynamic parameters obtained from a similar photobioreactor structure. A wide range of solar radiation conditions was covered (around 2 months of data with sunny and cloudy days), where the culture was operated in continuous mode at 0.34 l day^{-1}. The volumetric flow rate of air was constant at 140 l min^{-1}, allowing to capture the kinetic properties of the photosynthesis rate through the dissolved oxygen variable. The available data have been divided into two sets, one for calibration and another for validation purposes. Regarding CO_2 injections, an analysis on the pH was carried out in order to set up profiles of input signals that allow

to regulate the pH, avoiding damages to the culture, and at the same time, capturing dynamics related to CO_2 injection. Multilevel PRBSs were performed by a pulse-width modulation due to the discontinuous nature of the CO_2 valve, and these signals were adapted according to the period of day to keep the pH value in an appropriate and secure range (Sánchez et al. 2008a, b). Several data were registered remaining the volumetric flow rate around 30 l min^{-1}. Finally, the velocity of the culture flow was fixed at 1 m s^{-1} (notice that working with constant velocity is the typical way of operating these kinds of systems, although the developed model can cope with changing conditions on this variable).

4.1.1 Model Calibration and Validation

Regarding calibration and validation of the model, experimental data of solar radiation, biomass concentration, pH, and dissolved oxygen were required for calibration and validation steps. These problems were divided into two periods, night period when microalgae build up CO_2 due to respiration process, and light period when the photosynthesis rate is produced and CO_2 is consumed. Mass transfer parameters for the loop section (a_l and b_l, Eq. (21)) were calibrated with pH values (due to its higher influence on the CO_2 injections) during night periods, where the solar influence is neglected and therefore only mass transfers take place. In the presence of radiation, parameters like the light availability (both at the loop α_l and bubble column α_c), maximum photosynthesis rate, $P_{O_{2,max,t}}$, form parameters K_i and m_t, and the exponent, n_t, were adjusted using the dissolved oxygen, Eqs. (1) and (2), whereas mass transfer parameters for the bubble column (a_c and b_c, Eq. (22)) were calibrated by the difference between dissolved oxygen in the loop and in the bubble column, that is motivated by the influence of the air injection in the bubble column on the dissolved oxygen. On the other hand, respiration rate, Eq. (2), was established from results to 1% of the maximum photosynthesis rate. Furthermore, several measurements of biomass concentration were used to adjust biomass yield coefficient produced by the oxygen unit mass $Y_{o/x}$, Eqs. (4) and (5). The rest of parameters of Eq. (2) were maintained at values from laboratory scale, being necessary to perform aggressive test that limits the growth rate of the culture (close to limit conditions) to fit these parameters appropriately. Other parameters, such as tube diameter, culture heat capacity, tube length, etc., remained constants at values fixed by the design and previous knowledge of the system, and these parameters are shown in Tables 1 and 2.

Summarizing, the model is compound of two biological Eqs. (1) and (2), where a total of 14 characteristic parameters must be calibrated in real conditions, although six of them (z, K_{O_2}, B_1, C_1, B_2 and C_2), related to the factors of pH and dissolved oxygen, have remained at values from laboratory scale obtaining successful results. The rest of them (a_l, a_c, K_a, $P_{O_{2,max,t}}$, n_t, m_t, K_i, and r) have been calibrated by the procedure described in this work converging to an identifiable solution of these equations. Note that only the light availability parameter (a_l and a_c Eq. (1)) must be adjusted both for the solar receiver and for the bubble column due to the different solar exposition characteristics of each part. On the other hand, six mass balances (Eqs. (4),

Table 1 Common variables, constants, and characteristic parameters for both models

Parameter/Variable	Description	Value and units
B_1	Pre-exponential factors	2.4098
B_2	Pre-exponential factors	533.009
C_0	Drift flux model parameter	0.996
C_1	Activation energies	6.2684
C_2	Activation energies	68.8062
C_b	Biomass concentration	kg m^{-3}
$[CO_2^*]$	Equilibrium concentration with the gas phase for dioxide carbon	mol m^{-3}
$[CO_3^{2-}]$	Bicarbonate specie	mol m^{-3}
$[C_T]$	Total inorganic carbon concentration	mol m^{-3}
$[H^+]$	Hydrogen specie	mol m^{-3}
H_{CO_2}	Henry's constants for carbon dioxide	38.36 mol atm^{-1} m^{-3}
H_{O_2}	Henry's constants for oxygen	1.07 mol atm^{-1} m^{-3}
$[HCO_3^-]$	Carbonate specie	mol m^{-3}
I_{av}	Average solar irradiance	μE m^{-2} s^{-1}
I_0	Solar irradiance on an horizontal surface	μE m^{-2} s^{-1}
K_i	Form parameter	173.9504 μE m^{-2} s^{-1}
M_{CO_2}	Molecular weight of carbon dioxide	32 g mol^{-1}
M_{O_2}	Molecular weight of oxygen	44 g mol^{-1}
$[O_2]$	Dissolved oxygen concentration	mol m^{-3}
$[O_2^*]$	Equilibrium concentration with gas phase for oxygen	mol m^{-3}
Q_{gas}	Volumetric flow rate of gas	m^3 s^{-1}
Q_{liq}	Volumetric flow rate of liquid	m^3 s^{-1}
Q_m	Volumetric flow rate of culture medium	m^3 s^{-1}
t	Time	s
U_∞	Bubble accession rate	0.651 $m\ s^{-1}$
U_{gas}	Superficial velocity of the gas	0.0186 m s^{-1}
U_{liq}	Superficial velocity of liquid	0.0441 m s^{-1}
V_{mol}	Molar volume	20 L mol^{-1}
x	Longitudinal space along the loop	m
y_{CO_2}	Carbon dioxide molar fraction	
Y_{CO_2}	CO_2 to N_2 Molar ratio in gas phase	mol CO_2 (mol N_2)$^{-1}$
y_{O_2}	Oxygen molar fraction	
Y_{O_2}	O_2 to N_2 molar ratio in gas phase	mol O_2 (mol N_2)$^{-1}$
$Y_{o/x}$	Biomass yield coefficient	0.9713 kg $kg^{-1}O_2$
z	Form parameter	5.4333

Table 2 Variables, constants and characteristic parameters used into the tubular photobioreactor model

Parameter/Variable	Description	Value and units
a	Solar irradiance absorptivity	0.5411
a_c	Form parameters in the column	0.0806 s^{-1}
a_i	Interfacial area	m^{-1}
a_l	Form parameters in the loop	0.0012 s^{-1}
$A_{gas,l}$	Gas cross-sectional area of the loop	m^2
$A_{liq,l}$	Liquid cross-sectional area of the loop	m^2
$A_{t,c}$	Total cross-sectional area of the column	0.1257 m^2
$A_{t,l}$	Total cross-sectional area of the loop	0.0055 m^2
$A_{N_{2,l}}$	Cross-sectional area of the nitrogen gas in the loop	m^2
b_c	Form parameters in the column	0.7533
b_l	Form parameters in the loop	0.8450
$[CO_{2,p}]$	Carbon dioxide concentration in the liquid phase in the solar receiver	mol m^{-3}
$[C_T]_{m,t}$	Total inorganic carbon in the medium	8 mol m^{-3}
d_b	Bubble diameter	m
$d_{t,c}$	Total column diameter	0.4 m
$d_{t,l}$	Total loop diameter	0.084 m
$F_{N_{2,l}}$	Molar flow of nitrogen for gas phase in the loop	mol s^{-1}
$F_{N_{2,c}}$	Molar flow of nitrogen for gas phase in the bubble column	mol s^{-1}
$[HCO_3^-]$	Carbonate specie	mol m^{-3}
$K_{a,t}$	Extinction coefficient	133.0324 m^2 kg^{-1}
$K_{CO_{2,c}}$	Transfer coefficient constants for CO_2 in the column	0.91
$K_{CO_{2,l}}$	Transfer coefficient constants for CO_2 in the loop	0.91
K_l	Liquid-side mass transfer coefficient	m s^{-1}
$K_l a_{l,CO_2 c}$	Volumetric gas–liquid mass transfer coefficient for CO_2 in the column	s^{-1}
$K_l a_{l,CO_2 l}$	Volumetric gas–liquid mass transfer coefficient for CO_2 in the solar receiver	s^{-1}
$K_l a_{l,O_2 c}$	Volumetric gas–liquid mass transfer coefficient for O_2 in the column	s^{-1}
$K_l a_{l,O_2 l}$	Volumetric gas–liquid mass transfer coefficient for oxygen in the solar receiver	s^{-1}
$K_{O_{2,t}}$	Oxygen inhibition constant	0.7202 mol m^{-3}
m_t	Form parameter	0.0015
n_t	Form exponent	0.9779

(continued)

Table 2 (continued)

Parameter/Variable	Description	Value and units
$[O_2]_{m,t}$	Dissolved oxygen in the medium	0.2812 mol m^{-3}
$P_{CO_{2,t}}$	Carbon dioxide consumption rate	$kgCO_2$ kg^{-1} s^{-1}
$P_{O_{2,t}}$	Photosynthesis rate	kgO_2 kg^{-1} s^{-1}
$P_{O_{2,max,t}}$	Maximum photosynthesis rate	4.37E-05 kgO_2 kg^{-1} s^{-1}
P_T	Total pressure	1 atm
Q_w	Volumetric flow rate of water cross heat exchanger	m^3 s^{-1}
r	Respiration factor	0.01
V	Velocity of the fluid	1 m s^{-1}
$V_{liq,c}$	Liquid bubble column volume	m^3
$V_{gas,c}$	Gas bubble column volume	m^3
$V_{t,c}$	Total bubble column volume	0.4021 m^3
V_{ext}	Heat exchanger volume	20.3 L
$y_{N_{2,l}}$	Nitrogen molar fraction used in the solar receiver	
$y_{N_{2,c}}$	Nitrogen molar fraction used in the bubble column	
$Y_{o/x}$	Biomass yield coefficient	0.9713 kg $kg^{-1}O_2$
α_t	Distribution solar factor	
α_c	Distribution solar factor for bubble column	0.1052
α_l	Distribution solar factor for solar receiver	0.9725
ε_l	Gas holdup loop in the solar receiver	
ε_c	Gas holdup in the bubble column	

(6), (9), (11), (13), and (16)) for the solar receiver, and five mass balances (Eqs. (5), (8), (10), (12), and (14)) for the bubble column represented the temporal and spacial physicochemical phenomena that take place into the photobioreactors, where three parameters (a_l, b_l, and a) for the loop and two for the bubble column (a_c and b_c) have been calibrated.

Figure 5 shows some representative results of the calibration process, where both experimental and simulated concentrations of dissolved oxygen, pH, and biomass are shown. It can be seen how the model captures fast variations of the pH motivated by the CO_2 injections and the solar radiation, whereas smooth changes in dissolved oxygen and biomass concentration are also represented. As can be appreciated from Fig. 6, the model reproduces clearly the closed-loop nature of the system producing periodic oscillations related to the fluid velocity of the system, being one of the improvements reached with the use of PDE equations to model the transport phenomena respect to the model published in (Fernández et al. 2012). The calibration results showed mean errors between simulated and experimental data of 6.92 and

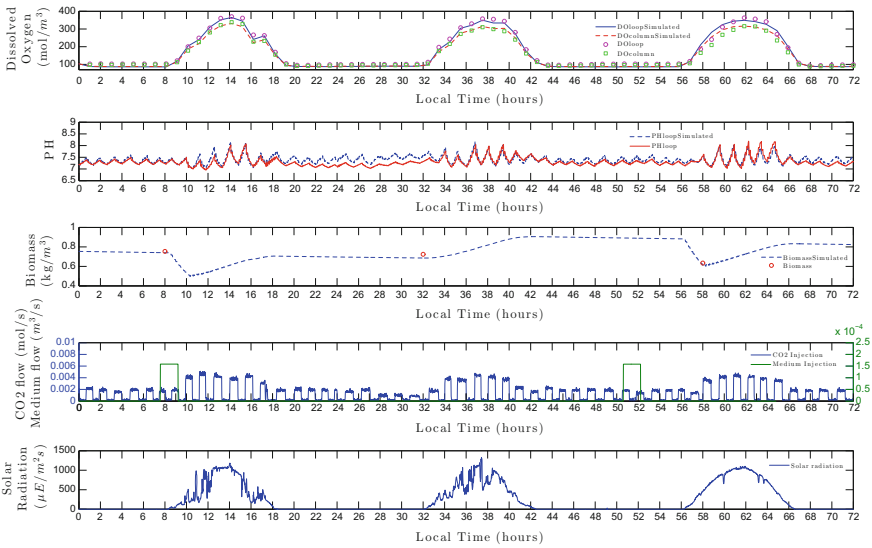

Fig. 5 Calibration results: Simulated and experimental data of dissolved oxygen concentration (DO), pH, and biomass concentration as a function of CO_2 injection and solar radiation (February 3, 4, and 5, 2014) (Fernández et al. 2014)

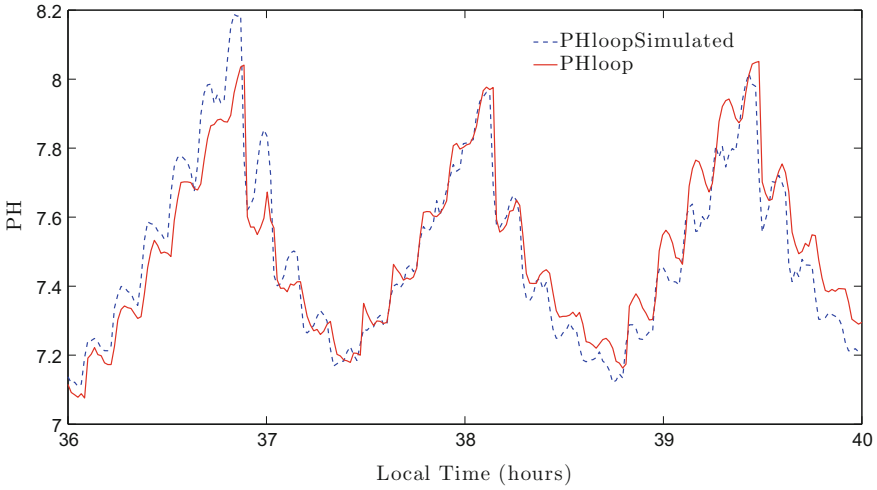

Fig. 6 Enlarged view of calibration results (Fernández et al. 2014)

4.99% for the dissolved oxygen (loop and bubble column, respectively), 1.65% for pH, and 3.44% for biomass concentration.

Figures 7 and 8 show similar results for the validation process, where an average of the parametric values obtained in the calibration process was considered (these

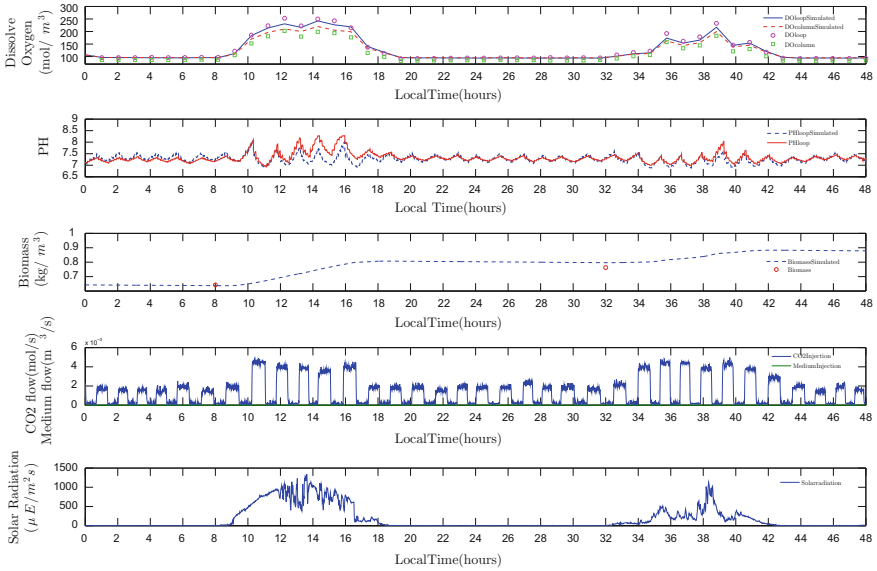

Fig. 7 Validation results: Simulated and experimental data of dissolved oxygen concentration (DO), pH, and biomass concentration as a function of CO_2 injection and solar radiation (February 25 and 26, 2014) (Fernández et al. 2014)

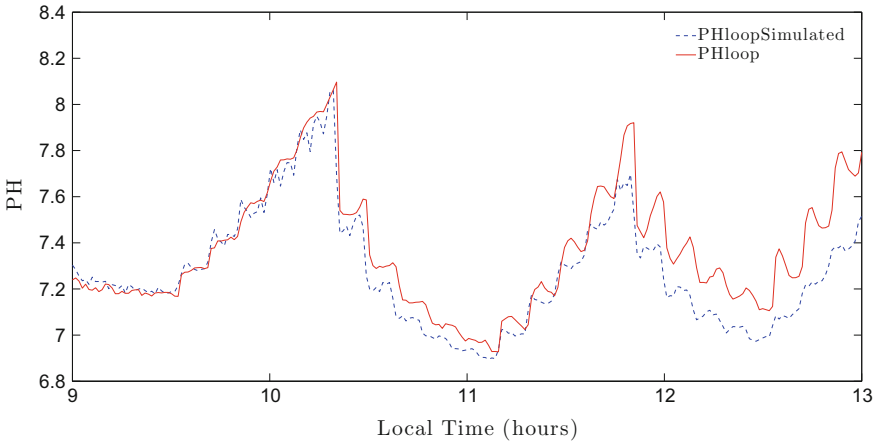

Fig. 8 Enlarged view of validation results (Fernández et al. 2014)

parameters are shown in Tables 1 and 2). The mean errors for this case were 3.43 and 10.81% for the dissolved oxygen, 1.56% for pH, and 2.81% for biomass concentration.

As observed from the calibration and validation results, the model properly fits the real data for the different process variables.

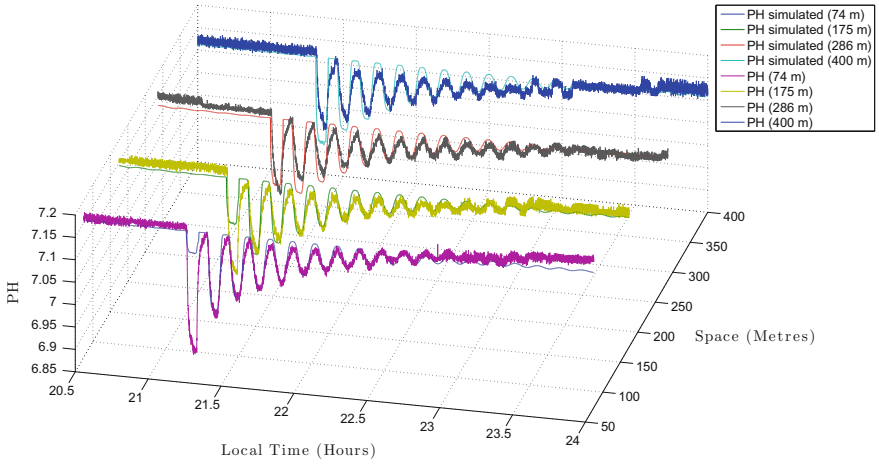

Fig. 9 Effects of a CO_2 pulse on the pH spatial distribution (Fernández et al. 2014)

4.1.2 Uses and Applications of the Model

In this section, some uses and applications are outlined. The previous results can be considered a good approximation to the main system dynamics from the input–output point of view. However, the model can be also used to analyze the behavior of the different variables along the loop in the reactor. Figure 9 shows a comparison between multiple measurement points located in different places of the loop. A CO_2 pulse was injected during the night (without solar irradiance) causing periodic oscillations due to the closed-loop nature of the system. It can be observed how the model reproduces this phenomenon, but the output of the model in the first cycle presents deviations from the real behavior mainly in the first sensors (those closer to the injection point). In view of these results, it can be concluded that in the first cycle, from the spatial point of view, the model should have to be improved by including molecular diffusion phenomena in the liquid phase to try to model this observed behavior (see Fernández et al. 2014).

On the other hand, the proposed model is able to predict the microalgal growth influenced by disturbances such as solar radiation and ambient temperature, which influence directly on the culture conditions (pH and dissolved oxygen). In addition to this, other system variables, which cannot be measured, are modeled such as carbon dioxide and total inorganic carbon concentration, oxygen, and carbon dioxide molar fraction in the gas phase, and even the carbon dioxide losses of the system. Moreover, relations between the culture conditions and the inputs broadly used in any kind of microalgal system are taken into account. The model can be considered as a useful tool in the optimization and design of photobioreactors, allowing to perform simulated studies for consecutive days both in discontinuous and continuous modes as can be seen in Fig. 7. Also, the proposed model can be used as a virtual sensor, allowing to predict unmeasured variables in a synchronous way to

the real plant and obtaining real-time estimations. From a control point of view, a dynamic first principle-based model provides a powerful tool to simulate any type of control strategies. Finally, since the model is based on physical, chemical, and biological principles, it can be also used to elaborate optimal or hierarchical control strategies. In these kinds of strategies, the problem is divided into layers where the upper layer is focused on the resolution of an optimization problem, while the lower layer manages the information provided from the upper layer in order to manipulate local regulators.

4.2 Results for Raceway Photobioreactor

In this section, the results for the raceway reactor are presented. The experimental data were obtained under normal operating conditions of the reactor (liquid velocity at 0.2 m s^{-1}, pH = 8 by injection of flue gas, semicontinuous operation at 0.2 day^{-1} dilution rate with volumetric flow rate of medium at 30 l min^{-1}) for different dates, covering a wide range of solar radiation conditions. Measurements of dissolved oxygen and pH at the end of each part of the reactor (channel, paddle wheel, and sump) were registered, in addition to environmental conditions (solar radiation, and temperature), and operation parameters (CO_2 injection, dilution of the culture). Initial values of characteristic parameters were obtained from previous knowledge. Thus, value of biological parameters such as the extinction coefficient ($K_{a,r}$), maximum photosynthesis rate ($P_{O_2,\max,r}$), form parameters (m_r, n_r, z), oxygen inhibition constants ($K_{O_2,r}$), pre-exponential factors (B_1, B_2), activation energies (C_1, C_2), and the respiration constant (R_{O_2}) were taken from (Costache et al. 2013). On the other hand, values of mass transfer coefficients for each part of the reactor were taken from Godos et al. (2014) and Mendoza et al. (2013b).

4.2.1 Model Calibration and Validation

To determine the real values of these characteristic parameters through the calibration and validation processes, data of dissolved oxygen and pH from the real reactor were compared with the output of the model using an optimization problem on the IAE error, an optimum value of these parameters being determined for each day used in the calibration procedure. Figure 10 allows to compare the real and simulated data obtained using the developed model. As observed, the model response fits the experimental data for both dissolved oxygen and pH. The model captures smooth variations of the photosynthetic rate produced by the bell-shaped form of the solar radiation. Increase of dissolved oxygen and pH due to photosynthesis by solar radiation availability is simulated. Changes produced through CO_2 injections, as pH and dissolved oxygen decrease, are also represented by the proposed model, taking into account the different dynamics taking place with and without the presence of solar radiation. Moreover, the model allows us observing how the characteristic delay of

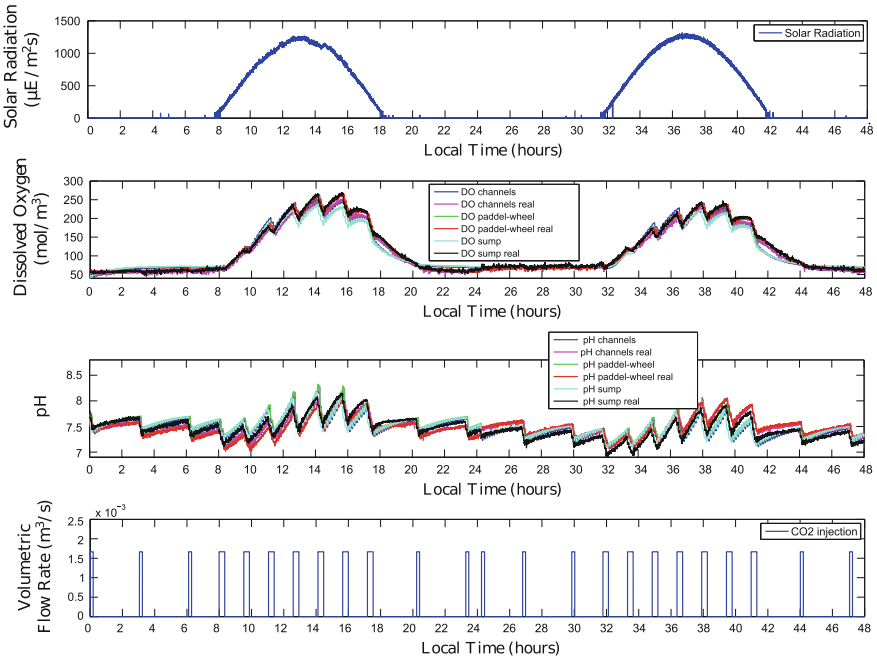

Fig. 10 Experimental and simulated data of dissolved oxygen concentration and pH at the end of the channels, paddle wheel, and sump. All of them as a function of CO_2 injection and solar radiation of two representative days used for model calibration purposes (Fernández et al. 2016)

the system produces an increase of pH and dissolved oxygen in the channels and paddle wheel, both variables decreasing after the sump. The mean errors between the simulated and experimental data were of 8.2, 8.6, and 10.0% for the dissolved oxygen at the end of the channel, paddle wheel, and sump, respectively, and of 1.5, 1.8, and 1.6% for the pH for the same sections.

As a result of the calibration procedure, the average values of characteristic parameters were determined (see Tables 1 and 3). Regarding biological parameters, the maximum photosynthesis rate was 2.06×10^{-5} kgO_2 kg^{-1} s^{-1}, whereas the extinction coefficient was 80 m^2 kg^{-1}, and the coefficients respiration rate (R_{O_2} and R_{CO_2}) were 9.58×10^{-7} kgO_2 kg^{-1} s^{-1} and 4.28×10^{-6} $kgCO_2$ kg^{-1} s^{-1} for oxygen and carbon dioxide, respectively. The rest of biological parameters being $n_r = 1.045$, $K_i = 174$ μ E m^{-2} s^{-1} and $m_r = 0.0021$. Regarding the volumetric mass transfer coefficients for oxygen in the different sections of the reactor, the values obtained were 2.5×10^{-6} s^{-1}, 2.2×10^{-3} s^{-1} and 6.3×10^{-3} s^{-1}, for channel, paddle wheel, and sump, respectively.

Validation of the model was performed to check the model quality, using a different set of data in different dates (validation data), in order to avoid possible bias and variance errors. For this validation process, the reactor was operated under the same conditions that in the calibration stage, where model includes the characteristic parameters obtained from calibration process being compared with experimental

Table 3 Variables, constants and characteristic parameters used into the raceway photobioreactor model

Parameter/Variable	Description	Value and units
$[CO_2]$	Carbon dioxide concentration in the liquid phase	mol m^{-3}
$[C_T]_{m,r}$	Total inorganic carbon in the medium	3 mol m^{-3}
h	Liquid height	0.17 m
h_w	Wall height	0.46 m
h_s	Solar hour	h
h_{ss}	Subterranean height of the sump	h
$K_{a,r}$	Extinction coefficient	80 m^2 kg^{-1}
$K_{laO_{2_{ch}}}$	Volumetric gas–liquid mass transfer coefficient for CO_2 in the channels	$2.5000 \cdot 10^{-6}$ s^{-1}
$K_{laO_{2_p}}$	Volumetric gas–liquid mass transfer coefficient for CO_2 in the paddle wheel	0.0219 s^{-1}
$K_{laO_{2_s}}$	Volumetric gas–liquid mass transfer coefficient for CO_2 in the sump	0.0063 s^{-1}
$K_{laCO_{2_{ch}}}$	Volumetric gas–liquid mass transfer coefficient for CO_2 in the channels	s^{-1}
$K_{laCO_{2_p}}$	Volumetric gas–liquid mass transfer coefficient for CO_2 in the paddle wheel	s^{-1}
$K_{laCO_{2_s}}$	Volumetric gas–liquid mass transfer coefficient for CO_2 in the sump	s^{-1}
$K_{O_2,r}$	Oxygen inhibition constant	0.8373 mol m^{-3}
l_s	Length of the sump	1 m
m_r	Form parameter	0.0021
N	Day of the year	d
n_r	Form exponent	1.045
$[O_2]_{m,r}$	Dissolved oxygen in the medium	0.2812 mol m^{-3}
P_b	Net production of biomass	kgO_2 kg^{-1}
$P_{CO_{2,r}}$	Carbon dioxide consumption rate	$kgCO_2$ kg^{-1} s^{-1}
$P_{O_{2,r}}$	Photosynthesis rate	kgO_2 kg^{-1} s^{-1}
$P_{O_{2,max,r}}$	Maximum photosynthesis rate	$2.06 \cdot 10^{-5}$ kgO_2 kg^{-1} s^{-1}
R_{O_2}	Respiration coefficient for dissolved oxygen	$9.58 \cdot 10^{-7}$ $kgCO_2$ kg^{-1} s^{-1}
Q_h	Volumetric flow rate during the harvesting process	m^3 s^{-1}
s_x	Shadow onto the surface of the cross-sectional area	m^2
V_r	Velocity of the fluid	0.2 m s^{-1}
V_p	Volume of the paddle wheel	0.1651 m^3
V_s	Volume of the sump	0.8151 m^3
w	Width of the channel	1 m

(continued)

Table 3 (continued)

Parameter/Variable	Description	Value and units
w_s	Width of the sump	0.9 m
y_{N_2}	Nitrogen molar fraction	
Y_{b/O_2}	Biomass yield coefficient	0.7273 kg
ε_s	Gas holdup in the sump	
α_s	Distributed factor	
α	Solar altitude angle	
δ	Sun declination	
ω	Solar hour angle	
ϕ	Latitude	
γ	Azimuth angle	
γ_0	Angle from North to the normal vector of the reactor	

data. Figure 11 shows how the simulation fits experimental results, the adequacy of the model to simulate experimental data being confirmed. The mean error for the dissolved oxygen was 4.9, 1.6, and 1.5% at the end of the channel, paddle wheel, and sump. On the other hand, the difference between the experimental pH of the culture and the simulated pH was 1.1, 1.0, and 1.2% for the same sections, proving an accurate response of the model for real conditions of operation.

It can be concluded that the proposed model captures the variations of the dissolved oxygen caused by the daily variation of solar radiation, and consequently of the photosynthesis rate. Furthermore, the model represents the transfer and consumption of carbon dioxide, thus allowing to simulate the variation of pH as a function of photosynthesis rate and CO_2 injections performed to feed the system and control the pH of the culture.

4.2.2 Uses and Application of the Model

Once the model has been calibrated and validated, it can be also used to simulate different designs, conditions, or scenarios (Fernández et al. 2016). For instance, the influence of the height of the reactor wall on the light availability can be analyzed. Figure 12 shows the influence of normal wall height of the reactor (h/h_{liq}) demonstrating that using walls with heights double than liquid reduces the productivity a 30%. As was expected, the optimal point was found in the unit of this relation, since on the contrary the difference between these heights generates shadows when the solar radiation is projected onto the surface of the liquid, producing a lower level of production. Once the wall height is optimized, the other relevant parameter is the water depth because it determines the light availability inside the culture through the average irradiance. Figure 13 shows the results obtained modifying the liquid height

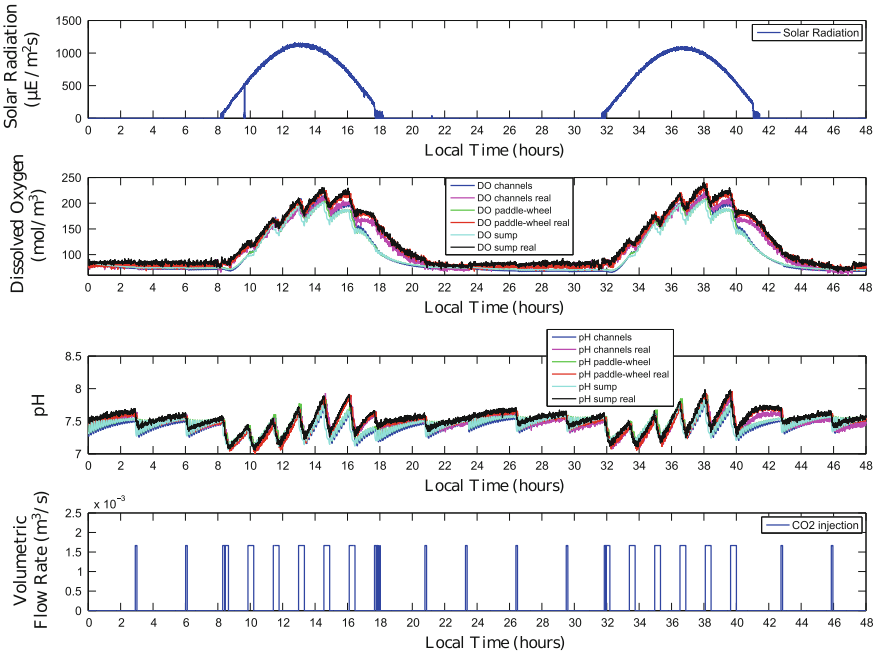

Fig. 11 Experimental and simulated data of dissolved oxygen concentration and pH as a function of CO_2 injection and solar radiation of two representative days used for validation purposes (Fernández et al. 2016)

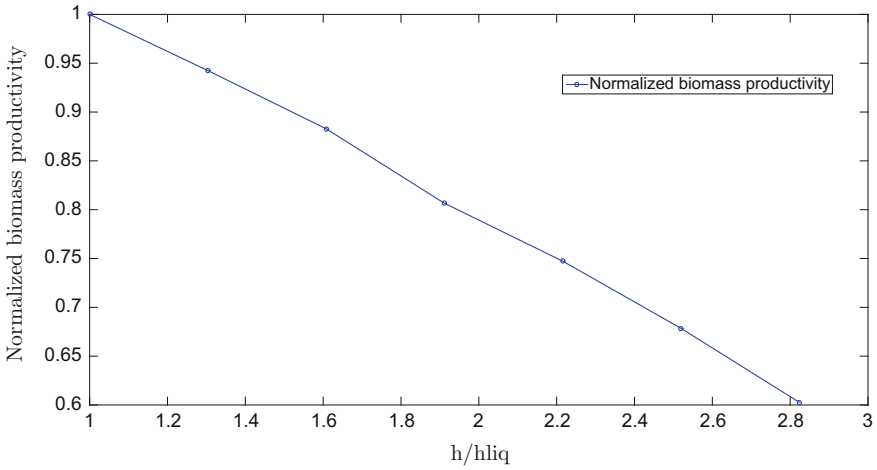

Fig. 12 Influence of normalized wall height on normalized biomass productivity of *Scenedesmus almeriensis* semicontinuous cultures in outdoor raceway reactor under standard conditions (Fernández et al. 2016)

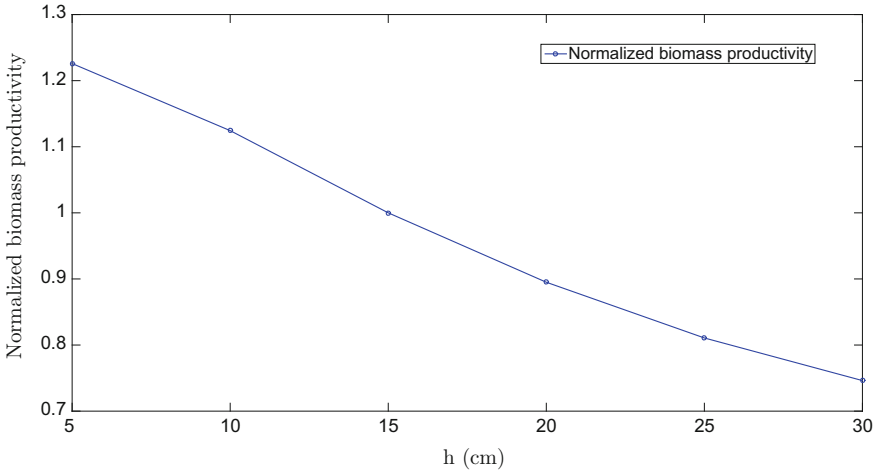

Fig. 13 Influence of water depth on normalized biomass productivity of *Scenedesmus almeriensis* semicontinuous cultures in outdoor raceway reactor under standard conditions (Fernández et al. 2016)

into the reactor but maintaining the rest of operational and design conditions (length and wide) of the reactor in any case. Note that in this case, the wall height and the liquid height have been established to equal values in order to avoid the negative effects produced by shadows in the system. Data show how the biomass productivity of the system exponentially increases when reducing the water depth, increasing 72% when the water depth reduces from 30 to 5 cm. It is important to note that these results do not consider the difficulty of operating large raceways at low water depth, as losses of efficiency on the paddle wheel or water depth variations along the reactor. Some other analysis, as the channel length, among others, can be done. See (Fernández et al. 2016) for a detailed analysis.

On the other hand, the developed model is a powerful tool for the study of existing raceway reactors producing microalgae biomass. Thus, from direct measurements of dissolved oxygen, pH, and CO_2 injection, it is possible to obtain the values of characteristic parameters of the system, both biological and engineering ones. Data obtained from calibration of the model versus experimental data agree with previously reported for this reactor (Godos et al. 2014; Mendoza et al. 2013a, b). The extinction coefficient of the biomass is in the range of 50–200 $m^2\ kg^{-1}$ reported for microalgae, whereas the photosynthesis rate is more than one order of magnitude higher than the respiration rate of $2.06 \cdot 10^{-5}$ and $9.58 \cdot 10^{-7}$ $kgO_2\ kg^{-1}\ s^{-1}$, respectively. The model also allows us to determine characteristic parameters of the growth model of the strain used (n_r, K_i, and m_r) that are usually determined at laboratory conditions, requiring long time and numerous experiments (Costache et al. 2013). Regarding the mass transfer coefficients determined from the calibration procedure, results agree with previously reported for the same reactor (Mendoza et al. 2013a), confirming that mass transfer mainly takes place in sump and paddle wheel. The

model confirms that channels perform as a "tubular reactor", where no relevant exchange of oxygen and CO_2 takes place between the culture and the atmosphere, besides the general knowledge that in raceway reactors oxygen accumulation does not take place and large CO_2 losses take place into the channel. Thus, the model allows us to demonstrate that oxygen is accumulated into the culture up to values of 0.4 mol/m^3 because the photosynthesis rate is higher than oxygen desorption capacity. On the opposite, the injected CO_2 is higher than CO_2 consumption by the cells, being mainly lost to the atmosphere into the sump and paddle wheel. However, CO_2 losses into the channels are three orders of magnitude lower. This behavior is analogous to that reported in tubular photobioreactors (Camacho et al. 1999). Then, it can be concluded that the design of both types of reactors, raceway and tubular, is not so different as usually reported.

Another interesting usage of the modes is to see that results here reported concerning the spatial–temporal variation of culture parameters demonstrate that static models cannot be used to adequately represent this type of reactors. Thus, microalgae have different responses (photosynthesis rate, etc.) to changes in the culture conditions not only along the day but also at the different positions inside the reactor (Fernández et al. 2012). Several studies reported dissolved oxygen concentrations in raceways as high as 500 %Sat., causing inhibition of photosynthesis and growth, and eventually leading to culture death (Marquez et al. 1995; Mendoza et al. 2013b; Singh et al. 1995; Vonshak 1997). Otherwise, it has also been reported that algal cultures in raceways can become carbon limited if only CO_2 from the air is available (Stepan et al. 2002), to maximize the productivity being necessary to maintain a CO_2 concentration in the bulk liquid of at least 65 μmol/L and a pH of 8.5 for high productivity of some microalgae (Weissman et al. 1988). To provide CO_2 and maintain the pH, it is possible to supply flue gases, but it is necessary to adequately design and operate the CO_2 supply unit (Godos et al. 2014). Moreover, the existence of pH gradients into the reactor reduces the performance of microalgae cultures (Berenguel et al. 2004; García et al. 2003). Experimental data here reported confirm the existence of relevant variations of culture conditions with time and position inside the reactor. Variation of culture parameters along the day is a consequence of solar daily variation, whereas variations along the different sections of the raceway is a consequence of the different rates of phenomena taking place (biological, physic, and chemical).

5 Conclusions

Two dynamic models based on first principles of the production of microalgae in raceway and tubular reactors have been developed, calibrated, and validated. The developed models have demonstrated to reproduce the spatial and temporal variations of main variables (light, biomass, dissolved oxygen, carbon dioxide, and pH) in tubular and raceway reactors, where biological and engineering aspects of the system are integrated. These models are useful tools to design and operate photo-

bioreactors in a conservative way, for the boundary conditions of maximum solar radiation availability or whatever other situation. However, as the model also allows us to include the variation with time of culture parameters, it can be used for the implementation of advanced control strategies, and to refine the design and operation of open reactors taking into account the dynamic accumulation or uptake of compounds, thus optimizing it. Dynamic models based on first principles as those here reported are a necessary and powerful tool for the improvement of industrial reactors.

Acknowledgements This work has been partially funded by the following projects: DPI2014-55932-C2-1-R (Spanish Ministry of Ecomony and Competitiveness and FEDER funds); EDAR-SOL CTQ2014-57293-C3 (Spanish Ministry of Science and Innovation); PURALGA RTA2013-0056-C03 (INIA), and supported by Cajamar Foundation.

References

Acién F, Fernández JM, Molina E (2013) Photobioreactors for the production of microalgae. Rev Environ Sci BioTechnol 12(2):131–151

Acién F, Fernández JM, Molina-Grima E (2013) Economics of microalgae biomass production. Biofuels from Algae 14:313–325

Acién F, García F, Sánchez J, Fernández J, Molina E (1998) Modelling of biomass productivity in tubular photobioreactors for microalgal cultures: effects of dilution rate, tube diameter and solar irradiance. Biotechnol Bioeng 58(6):605–616

Acién FG, Fernández JM, Molina-Grima E (2013) Photobioreactors for the production of microalgae. Rev Environ Sci Biotechnol 12:1–21

Acién FG, Fernández JM, Sánchez JA, Molina E, Chisti Y (2001) Airlift-driven external-loop tubular photobioreactors for outdoor production of microalgae: assessment of design and performance. Chem Eng Sci 56(8):2721–2732

Acién FG, García F, Chisti Y (1999) Photobioreactors: light regime, mass transfer, and scaleup. Prog Ind Microbiol 35:231–247

Acién FG, García F, Sánchez JA, Fernández JM, Molina E (1997) A model for light distribution and average solar irradiance inside outdoor tubular photobioreactors for the microalgal mass culture. Biotechnol Bioeng 55:701–714

de Andrade G, Berenguel M, Guzmán JL, Pagano D, Acién F (2016) Optimization of biomass production in outdoor tubular photobioreactors. J Process Control 37:58–69

Berenguel M, Rodríguez F, Acién FG, García JL (2004) Model predictive control of pH in tubular photobioreactors. J Process Control 14:377–387

Bernard O (2011) Hurdles and challenges for modelling and control of microalgae for CO_2 mitigation and biofuel production. J Process Control 21(10):1378–1389

Camacho F, Acién FG, Sánchez JA, García F, Molina E (1999) Prediction of dissolved oxygen and carbon dioxide concentration profiles in tubular photobioreactors for microalgal culture. Biotechnol Bioeng 62:71–86

Chisti MY, Moo-Young M (1987) Airlift reactors: characteristics, applications and design considerations. Chem Eng Commun 60(1–6):195–242

Concasa A, Pisua M, Caoa G (2010) Novel simulation model of the solar collector of biocoil photobioreactors for co2 sequestration with microalgae. Chem Eng J 157:297–303

Costache TA, Acién FG, Morales MM, Fernández-Sevilla JM, Stamatin I, Molina E (2013) Comprehensive model of microalgae photosynthesis rate as a function of culture conditions in photobioreactors. Appl Microbiol Biotechnol 97:7627–7637

Fernández I, Acién F, Berenguel M, Guzmán JL (2014) First principles model of a tubular photobioreactor for microalgal productio. Ind Eng Chem Res 53:11–121, 27:11–136
Fernández I, Acién FG, Fernández JM, Guzmán JL, Magán JJ, Berenguel M (2012) Dynamic model of microalgal production in tubular photobioreactors. Bioresour Technol 126:172–181
Fernández I, Acién FG, Guzmán JL, Berenguel M, Mendoza JL (2016) First principles model of a tubular photobioreactor for microalgal productio. Algal Res 17:67–78
García JL, Berenguel M, Rodríguez F, Fernández Sevilla JM, Brindley Alias C, Acién FG (2003) Minimization of carbon losses in pilot-scale outdoor photobioreactors by model-based predictive control. Biotechnol Bioeng 84:533–543
de Godos I, Mendoza JL, Acién FG, Molina E, Banks CJ, Heaven S, Rogalla F (2014) Evaluation of carbon dioxide mass transfer in raceway reactors for microalgae culture using flue gases. Bioresour Technol 153:307–314
Guterman H, Vonshak A, Ben-Yaakov S (1990) A macromodel for outdoor algal mass production. Biotechnol Bioeng 35:809–819
James SC, Boriah V (2010) Modeling algae growth in an open-channel raceway. J Comput Biol 17:895–906
Jupsin H, Praet E, Vasel J (2003) Dynamic mathematical model of high rate algal ponds (HRAP). Water Sci Technol 48:197–204
Kittler R, Darula S (2013) Determination of time and sun position system. Sol Energ 93:72–79
Koller M, Muhr A, Braunegg G (2014) Microalgae as versatile cellular factories for valued products. Algal Res 6:52–63
Marquez FJ, Sasaki K, Nishio N, Nagai S (1995) Inhibitory effect of oxygen accumulation on the growth of spirulina platensis. Biotechnol Lett 17:225–228
Mendoza JL, Granados MR, de Godos I, Acién FG, Molina E, Banks C, Heaven S (2013a) Fluid-dynamic characterization of real-scale raceway reactors for microalgae production. Biomass Bioenerg 54:267–275
Mendoza JL, Granados MR, de Godos I, Acién FG, Molina E, Heaven S, Banks CJ (2013b) Oxygen transfer and evolution in microalgal culture in open raceways. Bioresour Technol 137:188–195
Molina E, Fernández J, Acién FG, Chisti Y (2001) Tubular photobioreactor design for algal cultures. J Biotechnol 92(2):113–131
Molina E, Fernández Sevilla JM, Sánchez Pérez JA, García Camacho F (1996a) A study on simultaneous photolimitation and photoinhibition in dense microalgal cultures taking into account incident and averaged irradiances. J Biotechnol 45:59–69
Molina E, García F, Sánchez JA, Acién FG, Fernández JM (1996b) Growth yield determination in a chemostat culture of the marine microalgaisochrysis galbana. J Appl Phycol 8(6):529–534
Molina E, Sánchez JA, García F, Robles A (1993) Gas-liquid transfer of atmospheric CO_2 in microalgal cultures. J Chem Technol Biotechnol 56(4):329–337
Molina E, Sevilla JM, Pérez JA, Camacho FG (1996) A study on simultaneous photolimitation and photoinhibition in dense microalgal cultures taking into account incident and averaged irradiances. J Biotechnol 45(1):59–69
Norsker N, Barbosa MJ, Vermuë MH, Wijffels RH (2011) Microalgal production—a close look at the economics. Biotechnol Adv 29:(24–27)
Posten C (2009) Design principles of photo-bioreactors for cultivation of microalgae. Eng Life Sci 9:165–177
Sánchez JF, Fernández JM, Acién FG, Cerón MC, Pérez J, Molina E (2008a) Biomass and lutein productivity of scenedesmus almeriensis: influence of irradiance, dilution rate and temperature. Appl Microbiol Biotechnol 79(5):719–729
Sánchez JF, Fernández JM, Acién FG, Rueda A, Pérez J, Molina E (2008b) Influence of culture conditions on the productivity and lutein content of the new strain Scenedesmus almeriensis. Process Biochem 43(4):398–405
Singh DP, Singh N, Verma K (1995) Photooxidative damage to the cyanobacterium spirulina platensis mediated by singlet oxygen. Curr Microbiol 31:44–48

Spolaore P, Joannis-Cassan C, Duran E, Isambert A (2006) Commercial applications of microalgae. J Biosci Bioeng 101:87–96

Stepan D, Shockey R, Moe T, Dorn R (2002) Carbon dioxide sequestering using microalgae systems. US department of energy, Pittsburgh, PA, US FC26-98FT 40320

Vonshak A (1997) Spirulina: growth, physiology and biochemistry. In: Vonhask (ed) spirulina platensis (arthrospira): physiology, cell-biology and biotechnology. London:Taylor and Francis (43–65)

Weissman JC, Goebel R, Benemann JR (1988) Photobioreactor design: mixing, carbon utilization, and oxygen accumulation. Biotechnol Bioeng 31:336–344

Xin L, Hong-Ying H, Ke G, Ying-Xue S (2010) Effects of different nitrogen and phosphorus concentrations on the growth, nutrient uptake, and lipid accumulation of a freshwater microalga Scenedesmus sp. Bioresour Technol 101:5494–5500

Zuber N, Findlay JA (1965) Average volumetric concentration in two-phase flow systems. J Heat Transfer 87(4):453–468

Springer

http://www.springer.com/978-981-10-1949-4

Prospects and Challenges in Algal Biotechnology
Tripathi, B.N.; Kumar, D. (Eds.)
2017, XI, 326 p. 72 illus., 58 illus. in color., Hardcover
ISBN: 978-981-10-1949-4